Neurobiology of Disease

A Novel Transgenic Rat Model for Spinocerebellar Ataxia Type 17 Recapitulates Neuropathological Changes and Supplies *In Vivo* Imaging Biomarkers

Alexandra Kelp,[1,3] Arnulf H. Koeppen,[4] Elisabeth Petrasch-Parwez,[5] Carsten Calaminus,[2] Claudia Bauer,[1,3] Esteban Portal,[1,3] Libo Yu-Taeger,[1,3] Bernd Pichler,[2] Peter Bauer,[1,3] Olaf Riess,[1,3] and Huu Phuc Nguyen[1,3]

[1]Institute of Medical Genetics and Applied Genomics, [2]Laboratory for Preclinical Imaging and Imaging Technology of the Werner Siemens-Foundation, and [3]Centre for Rare Diseases Tübingen, University of Tübingen, 72076 Tübingen, Germany, [4]Department of Neuropathology and Neurology, Albany, New York 12208, and [5]Department of Neuroanatomy and Molecular Brain Research, Ruhr-University Bochum, 44787 Bochum, Germany

Spinocerebellar ataxia 17 (SCA17) is an autosomal-dominant, late-onset neurodegenerative disorder caused by an expanded polyglutamine (polyQ) repeat in the TATA-box-binding protein (TBP). To further investigate this devastating disease, we sought to create a first transgenic rat model for SCA17 that carries a full human cDNA fragment of the *TBP* gene with 64 CAA/CAG repeats (TBPQ64). In line with previous observations in mouse models for SCA17, TBPQ64 rats show a severe neurological phenotype including ataxia, impairment of postural reflexes, and hyperactivity in early stages followed by reduced activity, loss of body weight, and early death. Neuropathologically, the severe phenotype of SCA17 rats was associated with neuronal loss, particularly in the cerebellum. Degeneration of Purkinje, basket, and stellate cells, changes in the morphology of the dendrites, nuclear TBP-positive immunoreactivity, and axonal torpedos were readily found by light and electron microscopy. While some of these changes are well recapitulated in existing mouse models for SCA17, we provide evidence that some crucial characteristics of SCA17 are better mirrored in TBPQ64 rats. Thus, this SCA17 model represents a valuable tool to pursue experimentation and therapeutic approaches that may be difficult or impossible to perform with SCA17 transgenic mice. We show for the first time positron emission tomography (PET) and diffusion tensor imaging (DTI) data of a SCA animal model that replicate recent PET studies in human SCA17 patients. Our results also confirm that DTI are potentially useful correlates of neuropathological changes in TBPQ64 rats and raise hope that DTI imaging could provide a biomarker for SCA17 patients.

Introduction

The group of polyglutamine diseases contains nine members including spinocerebellar ataxia (SCA) 1, 2, 3, 6, 7, and 17, Huntington disease (HD), dentatorubropallidoluysian atrophy, and spinobulbar muscular atrophy (Zoghbi and Orr, 2000; Riley and Orr, 2006). The proteins involved in these diseases are ubiquitously expressed in the body but cause selective neurodegeneration. Here, we focused on generating an animal of spinocerebellar ataxia type 17, which is an autosomal dominantly inherited, neurodegenerative, late-onset disease caused by a polyglutamine expansion in the TATA-box-binding protein (TBP) (Nakamura et al., 2001). This deadly disease is characterized by ataxia, dystonia, and seizures (Rolfs et al., 2003), as well as dementia, psychiatric and extrapyramidal features, epilepsy, mild sensorimotor axonal neuropathy, and MRI findings of cerebral and cerebellar atrophy (Maltecca et al., 2003). In contrast to most of the other polyQ disease causing proteins, the function of the TBP in the transcription process is well understood (Burley and Roeder, 1996) and potentially allows us to investigate how the mutation alters protein function subsequently leading to neuronal dysfunction *in vivo*.

Although two transgenic mouse models (Friedman et al., 2007; Chang et al., 2011) and one knock-in mouse model (Huang et al., 2011) already exist, which all mimic several phenotypic characteristics of the disease, mouse models are in general limited for studying certain functional and behavioral measurements (Tecott and Nestler, 2004; Rodriguiz and Wetsel, 2006; Herrmann et al., 2012). Rats, on the other hand, show excellent learning abilities compared to mice and are the species of choice for studying learning and memory in rodents and for pharmacological manipulations (Kujpers, 1999). Their larger brain size also facilitates direct invasive procedures and miniaturized physiological *in vivo* approaches such as structural and functional imaging of small brain structures (Casteels et al., 2011; Grundmann et al., 2012; Yu-Taeger et al., 2012), electrophysiology (Miller et al., 2010; Ortiz et al., 2012), or stem cell replacement (Rath et al., 2012; Ribeiro et al., 2012). The advantages of the rat prompted us to generate a transgenic rat model for SCA17, which, to our knowledge, is the first transgenic rat model for any inherited

Received Dec. 10, 2012; revised March 18, 2013; accepted April 9, 2013.

Author contributions: A.K., P.B., O.R., and H.P.N. designed research; A.K., A.H.K., E.P.-P., C.C., C.B., and L.Y.-T. performed research; A.K., C.C., E.P., and B.P. analyzed data; A.K., A.H.K., E.P.-P., C.C., and H.P.N. wrote the paper.

This work was supported by the RATstream Project (European Union Contract LSHM-03784). We are grateful for excellent technical assistance of Marlen Löbbecke-Schumacher, Hans-Werner Habbes, Celina Tomczak, and Therese Stanek.

Correspondence should be addressed to Dr. Huu Phuc Nguyen, Institute of Medical Genetics and Applied Genomics, University of Tübingen, Calwerstrasse 7, 72076 Tübingen, Germany. E-mail: hoa.nguyen@med.uni-tuebingen.de.

DOI:10.1523/JNEUROSCI.5622-12.2013

 0270-6474/13/339068-14$15.00/0

spinocerebellar ataxia. In line with previous observations in mouse models for SCA17, our transgenic SCA17 rats (TBPQ64; carrying a full human cDNA fragment of the TBP gene with 64 CAA/CAG repeats) show disease characteristic neuropathology such as neurodegeneration in the cerebellum and the formation of nuclear TBP accumulation as well as a severe neurological phenotype including ataxia, reduced activity, loss of body weight, and early death. Additionally, we were able to perform positron emission tomography (PET) and diffusion tensor imaging (DTI) measurements *in vivo* in our rat model and detected changes that were unreported in SCA17 patients so far. The accurate replication of the human condition in our TBPQ64 rats, coupled with the possibility to develop *in vivo* imaging biomarkers, makes this SCA17 rat model highly suited for the assessment of different interventions on the disease phenotype.

Materials and Methods

Generation of transgenic TBPQ64 rats

To generate transgenic SCA17 rats, we used a construct containing a fragment of the murine prion promoter (Prp), an N-terminal myc tag, full-length human TBP cDNA, and a poly-A tail (Fig. 1*A*).

The human TBP cDNA was amplified from TBP mRNA obtained from genomic DNA and cloned (XhoI/BamHI) into the Bluescript vector pBSSKII+. In this vector, we first cloned a 3.4 kb fragment of the murine prion protein promoter containing 1140 bp of the murine prion protein gene upstream of exon 1, the complete exon 1, intron 1, and the first untranslated 52 bp of exon 2. The promoter fragment was amplified by PCR using the primers phg_Prp_Xba_FP (5′-GCTCTAGAGCCAATCTTGTGTCTGG-3′) and phg_Prp_Bam_RP (5′-CGGGATCCCGGAATGCTTCAGCTCGG-3′). Both primers contain recognition sequences for the restriction enzymes XbaI and BamHI, which were used for the cloning of this fragment into the pBSSKII+ vector. Constructs were additionally tagged N-terminally with an myc tag. The 36 CAG/CAA repeat region was expanded to 38 as well as 64 repeats as described previously (Laccone et al., 1999). The construct was completed with a SV40 polyadenylation signal. After digestion with NeaI and NotI, the inserts were isolated before microinjection in Sprague Dawley oocytes.

Genotyping

After weaning, transgenic rats were identified by using a transgene-specific PCR protocol. Rat genomic DNA was isolated from rat ear biopsies according to the High Pure PCR Template Preparation Kit protocol (Roche). For the identification of transgenic animals, a PCR protocol with a forward primer from the mouse prion promoter (mTBP_F, 5′-gaaccatttcaaccgagctg-3′) and a reverse primer targeting the hTBP cDNA (mTBP_R, 5′-gtccaatgatgccttatggc-3′) was established. A 189 bp fragment was amplified using the following PCR conditions: 95°C, 30 s for denaturation; 60°C, 30 s for primer annealing; and 72°C, 30 s for elongation, repeated for 35 cycles.

Fragment length analysis

To determine the number of CAG/CAA repeats in the TBP transgene, fragment length analysis of DNA samples was performed. PCRs were performed to amplify a fragment of TBP containing the CAG/CAA repeat by using the following primers: 5′-Cy5-gaccccacagcctattcaga-3′ and 5′-ttgactgctgaacggctgca-3′. The indodicarbocyanine (Cy5)-labeled PCR products were mixed with an internal standard (DNA-Size Standard Kit-600; Beckman Coulter) and separated as well as analyzed on the CEQ8000 Genetic Analysis System (Beckman Coulter).

Plasmid DNA of TBP cDNA containing 13, 38, 64, or 105 CAG repeats was used as a size standard to calculate the number of CAG/CAA repeats.

Animals

Rats were housed in gender- and genotype-matched groups of up to four, according to Federation of European Laboratory Animal Science Associations recommendations (Rehbinder et al., 1996). All rats were kept under a 12 h light/dark cycle with lights on at 2 A.M.; food (Sniff lab chow pellets) and tap water available *ad libitum*.

For behavioral tests, predominantly male heterozygous and wild-type littermate control rats from litters were used. Two to four rats of randomized genotype were housed together. All rats were tested within the dark phase of a 12 h light/dark cycle. The ataxia score test was conducted in the light cycle, whereas the rotarod, beam walking, and elevated plus maze (EPM) tests were done in dark phase. All research and animal care procedures were approved by the district government (HG9/10, Tübingen, Germany) and performed according to international guidelines for the use of laboratory animals.

Behavioral tests

Before the experiments, animals were handled daily for 2 weeks. Furthermore, animals were weighted weekly. The numbers of animals in the behavioral studies as as follows: TBPQ64 males, $n = 12$; wild-type males, $n = 7$; TBPQ64 females, $n = 4$; wild-type females, $n = 8$.

Ataxia score test. This test was established by Guyenet et al. (2010) and facilitates rapid and sensitive quantification of disease severity in rodent

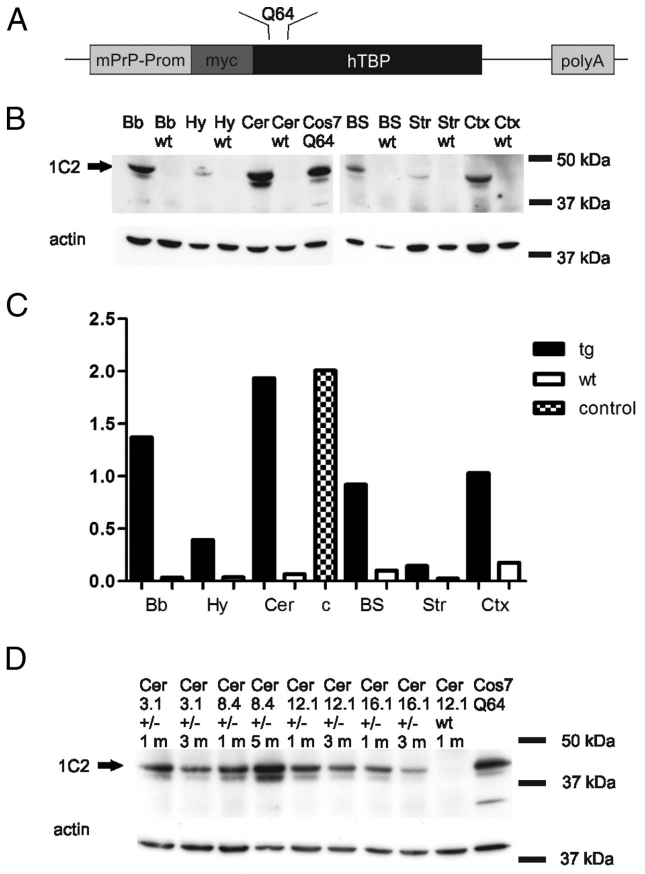

Figure 1. Construct and expression pattern of mutant TBP. ***A***, The TBP construct contains full-length human cDNA of the TBP gene with 64 CAG repeats under the control of the murine prion protein promoter (Prp-TBPQ64) and an N-terminal myc-tag. ***B***, Western blots of 5-month-old rats showing the expression pattern of mutant TBP in different brain regions (Bb, olfactory bulb; Hy, hypothalamus; Cer, cerebellum; BS, brainstem; Str, striatum; Ctx, cortex; wt, wild type). Mutant TBP is expressed in all analyzed regions; however, the highest level was found in the cerebellum. The arrow indicates mutant TBPQ64. ***C***, Quantification of the Western blot shown in ***B***. Black bars represent the transgenic samples (TBP Q64), and white ones the wild-type control. The checked bar is the positive control (transiently transfected Cos7 cells with the TBPQ64 construct). c, Control (Cos7 cells transiently transfected with TBPQ64). ***D***, Western blot of cerebellum samples of four different TBPQ64 lines at the ages of 1 and 3 months (line 8.4 at 5 months) using 1C2 antibody. The expression of mutant TBP differed significantly between the lines. The highest expression was found in line 8.4, and the lowest in line 16.1. As a positive control lysates from Cos7 cells transiently transfected with TBPQ64 were used. The arrow indicates mutant TBPQ64.

models of ataxia. The protocol includes the ledge test, measurement of hindlimb clasping, and assessment of gait abnormalities and severity of kyphosis. For each parameter we used a scale of 0–3 leading to a maximum value of 12 points for all four measurements. Because of the bigger size of rats, the ledge test was performed on a thin beam (width, 1 cm) instead of the cage ledge. The scoring was performed as described (Guyenet et al., 2010).

Rotarod analysis. This test is widely used to analyze balance capabilities, motor coordination, as well as motor learning of rodents. Seven wild-type animals and 12 transgenic rats were tested at the ages of 1, 3, 5, and 8 months. Rats were trained for 3 d on an accelerating rotarod (Ugo Basile; Biological Research Apparatus). Each training day consisted of four trials, with each trial lasting for 2 min. During the first 30 s, the rod accelerated from 2 to 12 rpm and then operated constantly for 1.5 min at 12 rpm. Rats that fell during this time period were immediately set back on the rod. On the two testing days, only two trials of 5 min duration were performed. Within the first 4 min, the rod accelerated from 4 to 40 rpm and then operated constantly at 4 rpm for the last min. The amount of time that elapsed before the rat fell off the rod was recorded. The mean of all four test runs was taken for analysis.

Beam walking. With the beam-walking test, motor coordination and balance of rats were assessed by measuring the ability of animals to traverse a series of narrow beams to reach an enclosed safety platform. The test was performed as described previously (Korenova et al., 2009) and consisted of two training and three testing days. On Training Day 1, the animals (7 wild-type, 12 transgenic males) underwent two trials in which they had to traverse a 2 m long beam with a square cross-section of 3 × 3 cm. On Training Day 2, two trials were given, one where they had to traverse the 3 × 3 cm beam, and one trial where a beam with a rectangular cross-section of 4 × 2 cm had to be crossed. On all three testing days, the rats had to cross each beam (3 × 3 cm and 4 × 2 cm in diameter, respectively, and a round beam of 3.5 cm diameter) once. Traversing latency and number of hind-limb slips during test performance were measured and analyzed.

Elevated plus maze. This well-established test is used to evaluate anxiety in small rodents. It is based on the aversion of rodents to open spaces and height. The setup consists of four elevated arms that built a plus shaped cross. Two opposing arms are open, and the other two arms are enclosed by 40 cm high walls; the width of the arms is 25 cm, and the distance from the floor is 80 cm. The test was performed in the dark phase in a room that was illuminated by a red rope light positioned directly above the maze. The experiment was started by placing the rat on the central platform, with its head facing one of the open arms. The time spent on the open arms during a 5 min period as well as the transitions between the center and the closed arms or the open arm were recorded. After each rat exposure, the maze was carefully cleaned with disinfectant.

The following parameters were calculated for a total trial duration (TT) of 300 s: duration of stay in closed arms [closed time (CLT)], percentage share of CLT in total arms-stay duration (%CLT; CLT × 100/TT), duration of stay in open arms [open time (OT)], percentage share of OT in total arm-stay duration (%OT; OT × 100/TT), duration of stay in the neutral zone [neutral time (NT)], and percentage share of NT in total arm-stay duration (%NT; NT × 100/TT).

PhenoMaster system. The TSE PhenoMaster system (http://www.tse-systems.com/products/behavior/phenomaster/index.htm) is an automated cage system that allows behavioral and metabolic monitoring, e.g., activity, food and water consumption, as well as calorimetric measurements. The system consists of a combination of sensitive feeding and drinking sensors for automated online measurements. Values for cumulative amounts of feeding and drinking were given by the system, and these were used to compare iterative food and water intake. The calorimetric system is an open-circuit system that determines O_2 consumption, CO_2 production, and respiratory exchange rate. To investigate locomotor activity, a photobeam-based activity monitoring system detects and records the number and duration of every total, fine, and ambulatory movement including rearing (Urbach et al., 2010).

In detail, rats were singly housed in a home cage equipped with the technical requirements to individually monitor one rat per cage at a time. The system was set up to measure up to 12 animals in parallel with high resolution for food and water consumption, calorimetric parameters, and activity. This allowed the measurement of fine and ambulatory movement as well as rearing behavior. Results for locomotor activity are given as number of counts, and all measurements were monitored using PhenoMaster software, version V1.9.20-06/2007 (TSE Systems).

Further analysis binned the exploratory phase in the first 20 min for the purpose of isolating animal activity before adaptation to the new environment. From these we calculated periphery to center ambulation ratio.

Animals (nine wild-type vs nine heterozygous males) were tested every second month for 72 h starting at the age of 3 and ending at 9 months.

Immunohistochemistry

Light microscopy on paraffin sections. Immunohistochemistry was performed as described previously (Boy et al., 2009). Transgenic and wild-type rats of both sex were investigated at the ages of 3 and 10 months. Antibodies were used at the following dilutions: 1C2 (clone 5TF1-1C2; Millipore), 1:5000; anti-β-III tubulin (clone TuJ-1, MAB1195; R&D Systems), 1:1000; and anti-myc (SA-294, clone 9E10; Biomol), 1:350.

Paraffin sections from human brains were treated like described previously (Koeppen et al., 2011). Sections were incubated in citrate buffer (0.01 M, pH 6.0) for 20 min at 90°C and stained with 1C2 (Millipore Bioscience Research Reagents), α-TBP (clone 1TBP18, 70102; QED Bioscience), and anti-β-III tubulin (clone TuJ-1, MAB1195; R&D Systems), respectively.

Light and electron microscopy on epoxide embedded vibratome sections. Male TBPQ64 and wild-type littermates, 9 months of age, were transcardially perfused with 4% PFA, embedded into 2% agarose, and cut into series of 50 μm vibratome slices from blocks containing the striatum and cerebellum. Every fifth section was taken either for light- and electron-microscopical TBP (1:5000) or calbindin D28 immunohistochemistry (1:10,000; No. 300, monoclonal; Swant) according to an avidin-biotin-peroxidase complex protocol as described previously (Petrasch-Parwez et al., 2007). For semithin and ultrathin section analysis, immunostained vibratome slices were postfixed with 2% osmium tetroxide in 0.1 M phosphate buffer, dehydrated, and flat-embedded in Araldite (Serva). Alternating semithin (0.8 μm) and ultrathin (100nm) section series were cut with a Leica Ultracut UCT microtome. Every second semithin section was slightly counterstained with 1% toluidine blue, and ultrathin sections were contrasted with 5% aqueous uranyl acetate followed by lead citrate.

Western blot analysis

Preparation of samples was performed as described previously (Boy et al., 2009). The 1C2 antibody (clone 5TF1-1C2; Millipore) was used at a concentration of 1:4000.

Secondary antibody anti-mouse HRP (NXA931; GE Healthcare) was diluted 1:2500.

PET analysis

For the PET experiments, female transgenic TBPQ64 ($n = 6$) and control rats ($n = 6$) were imaged using an Inveon dedicated small-animal PET scanner (Siemens Preclinical Solutions), yielding a spatial resolution of about 1.3 mm in the reconstructed image. Rats were lightly restrained and injected with 29.6 MBq [^{11}C]raclopride via a lateral tail vein. A 60 min dynamic PET scan was obtained immediately after tracer injection followed by a 15 min attenuation correction. During imaging, the animals were anesthetized with a mixture of 1.5% isoflurane and 100% oxygen. The animals were centered in the field of view of the PET scanner. Anesthesia was monitored by measuring respiratory frequency, and the body temperature was kept at 37°C by a heating pad underneath the animal. PET data were acquired in list mode, graphed in time frames of 4 × 60 s, 4 × 120 s, 8 × 300 s, and 2 × 450 s, and reconstructed using filtered backprojection algorithm with a matrix size of 256 × 256 and a zoom factor of two. Image files were analyzed using PMOD and AsiPro software (Siemens Preclinical Solutions). The PMOD image fusion software allowed linear transformation and rotation to overlay PET and MR template images. The PET/MR fusioned images were used to calculate specific regions of interest in different brain areas with reference to the stereotactic brain atlas of Franklin and Paxinos (2001). With the PMOD

software we also analyzed the [^{11}C]raclopride uptake in various brain areas including cerebellum, orbitofrontal cortex (OFC), and striatum. As a reference region, the cerebellum was chosen to correlate the unspecific uptake with the tracer uptake in the striatum and the OFC.

DTI measurements

Male transgenic rats as well as wild-type littermates were measured using DTI at 10 months ($n = 6$ for TBPQ64; $n = 3$ for WT) and 5 months of age ($n = 3$ for TBPQ64; $n = 3$ for WT). The images were produced using a Clinscan 7T MR scanner (Bruker BioSpin and Siemens Medical Solutions) and a four-channel rat brain surface coil. Rats were anesthetized using isoflurane with an induction of 2.5% and maintenance at 1.5%. Temperature and breathing rate were monitored throughout the studies, with a constant temperature at 37 ± 0.5°C. The measurements lasted ~60 min. Diffusion tensor images were acquired using an echo planar imaging with 256 directions [$b = 0$; 1000 s/mm^2; field of view (FOV), 54 × 21 mm; matrix, 128 × 52 mm; 26 1 mm slices; TE, 60 ms; TR, 5500 ms]. An anatomical T2-weighted image was also produced (matrix, 256 × 161 mm; FOV, 35 × 57 mm; TR, 3000 ms; TE, 205 ms; slice thickness, 0.22 mm). Fractional anisotropy (FA), radial diffusivity, diffusion weighted images, and apparent diffusion coefficient (ADC) maps were generated using DTI Studio software. PMOD software was used for the coregistration of the maps to the anatomical image, where a region of interest approach was implemented on the different parts of the striatum [dorsomedial (DMS) and ventral (ACB), substantia nigra (SN), and external capsule] using the following Paxinos coordinates: DMS, AP, −0.4 mm; ML, ±2.6 mm; DV, −5.0 mm; ACB, AP, +3.4 mm; ML, ±1.9 mm; DV, 5.3 mm; SN, AP, −4.8 mm; ML, ±2.0 mm; DV, −8.5 mm.

Statistical analysis

Data were analyzed by using GraphPad Prism 5. All results are shown as mean ± SEM. Results were regarded as significant with a p value <0.05.

Student's t test (for the EPM analysis) and two-way ANOVA for repeated measurements with a Bonferroni posttest were performed. We analyzed the interaction between age and genotype for all the other behavioral tests as well as for the weight measurement.

Results

Generation and first characterization of SCA17 rats

To generate SCA17 rats, we used a cDNA encoding human full-length TBP with a poly-glutamine stretch of 64 CAG/CAA repeats under the control of the murine prion promoter (PrpTBPQ64) (Fig. 1*A*). This promoter was used previously to drive expression of mutant ataxin-3 in a SCA3 transgenic mouse model with a cerebellar phenotype (Bichelmeier et al., 2007). After injecting the transgenic construct into fertilized Sprague Dawley oocytes, we received 64 pups. Ten of these 64 animals carried the transgene as determined by PCR. However, three potential founders died prematurely without any offspring, and two animals did not transmit the transgene to their offspring. Therefore, only in the remaining five lines the expression pattern of mutant TBP (mTBP) was analyzed by Western blot analysis. mTBP was detected in the cerebellum of all analyzed lines, with line 8.4 showing the highest expression level (Fig. 1*D*). Based on this, we chose line 8.4 for further characterization. Western blot analyses showed that these animals express mutant TBP predominantly in the cerebellum, with moderate levels of mTBP in the olfactory bulb and cortex, whereas the hypothalamus, brain stem, and striatum displayed only very low levels of mTBP (Fig. 1*B*,*C*), respectively. To verify the conservation of the CAG/CAA repeat in the mutant TBP cDNA of TBPQ64 rats, we analyzed the PCR fragment length of DNA samples from transgenic rats. We found that the CAG/CAA repeat is stable for at least three generations (data not shown), which is in line with observations in SCA17 patients (Tomiuk et al., 2007). Additionally, using the same construct only with 38 CAG/CAA repeats, transgenic rats bearing human TBP with a normal polyglutamine tract were generated.

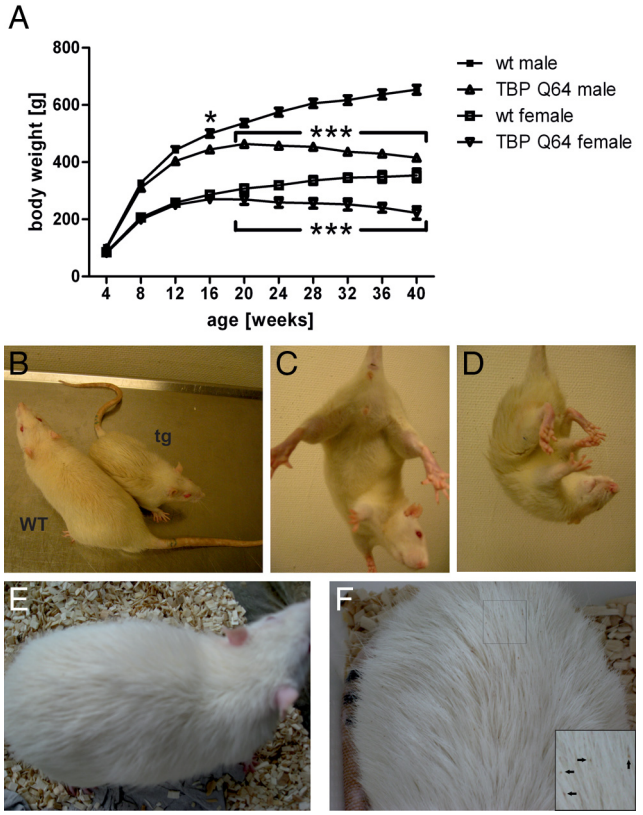

Figure 2. Phenotype of SCA17 rats. ***A***, Starting with 4 months of age, transgenic (tg) male rats ($n = 20$) had a significantly lower body weight than age-matched control animals ($n = 22$). In female rats, this body weight difference was observed at the age of 5 months [$n = 4$ for TBPQ64; $n = 8$ for wild-type (wt) rats]. *$p < 0.05$; ***$p < 0.001$. ***B***, At the age of 8 months, transgenic male rats were easily distinguishable from their wild-type littermates, as they were leaner and much smaller in size. ***D***, Clasping behavior is observed in TBPQ64 rats at the age of 8 months when suspended by the tail, whereas nontransgenic animals showed normal spreading behavior of the hindlimbs (***C***). ***E***, ***F***, Compared to control animals (***E***) heterozygous rats were poorly groomed (***F***) and had brownish, eschar resembling structures in the fur (arrows in the magnified inset).

While 2 lines of TBPQ38 rats were established, these rats did not showing any phenotypic abnormalities during their normal life span and were indistinguishable from the wild-type littermates (data not shown). This is expected as it has been shown for mice carrying TBP with a normal polyQ tract of 13 (Friedman et al., 2007). Therefore, here we show only data on TBPQ64 rats and their wild-type littermates.

Decreased body weight and a severe neurological phenotype in SCA17 rats

At birth and for the first 3 months of age, TBPQ64 rats appeared normal compared to their wild-type littermates. However, starting at 4 months of age, transgenic male rats had a significantly lower body weight than age-matched controls (Fig. 2*A*). This significant decrease of body weight was also observed in female TBPQ64 rats. Notably, TBPQ64 rats not only failed to gain weight after 5 months of age, but also showed a loss of body weight thereafter. On the other hand, wild-type animals continued to gain weight as expected. At the age of 8 months, TBPQ64 rats were highly phenotypic and easily distinguishable from control animals: they were cachectic, substantially smaller in body size when compared to wild types (Fig. 2*B*), and exhibited a hunched posture (kyphosis), poor grooming (Fig. 2*F*), and tremor. When suspended by the tail, these rats showed abnormal postures com-

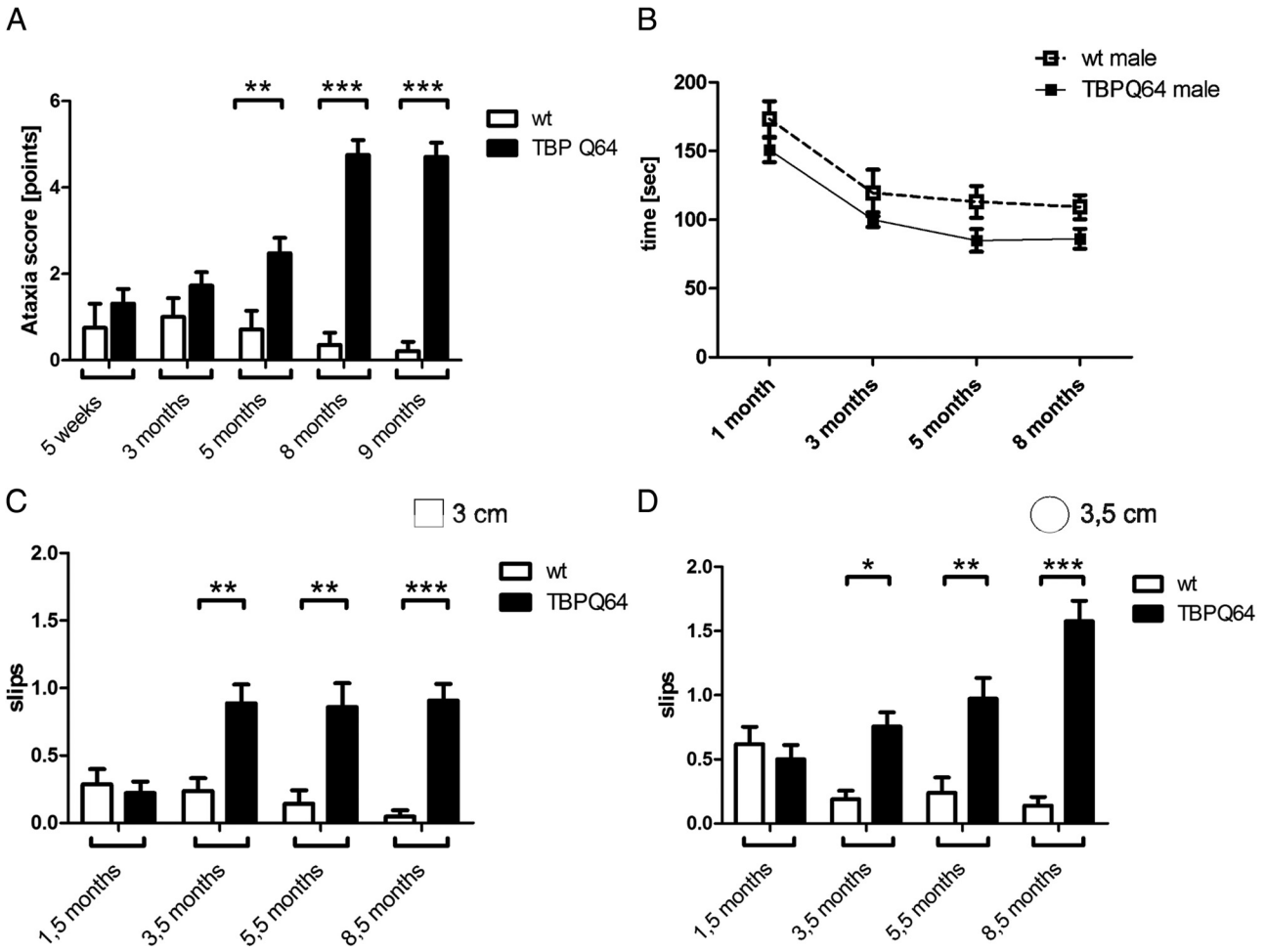

Figure 3. Neurological phenotype of SCA17 rats. ***A***, The ataxia score consists of four parameters (ledge test, hindlimb clasping, gait, and kyphosis). For each parameter, a score of 0–3 is given so that in total a maximum score of 12 points can be reached. Significant differences between TBPQ64 rats and wild-type (wt) littermates were observed in old transgenic animals (black columns), which presented clear atactic symptoms. ***B***, The rotarod performance decreased with age, but there were no significant differences between controls (black line) and transgenic animals (dotted line). ***C***, ***D***, The beam-walking test was performed at 1.5, 3.5, 5.5, and 8.5 months of age. Transgenic rats (black columns) showed a significant higher rate of slips on the 3 cm square beam (***C***), as well as on a round beam with 3.5 cm diameter (***D***). TBPQ64 rats exhibited a progressive decline in beam-walking ability with age. All tests were performed with male rats ($n = 7$ controls; $n = 12$ TBPQ64 rats). $^{*}p < 0.05$; $^{**}p < 0.01$; $^{***}p < 0.001$.

parable to clasping (Fig. 2*D*), whereas wild-type animals demonstrated normal escape reflexes with hindlimbs spread widely (Fig. 2*C*). At the age of 10 months, transgenic male TBPQ64 rats weighed, on average, 35% less than age-matched control animals even though they were additionally fed with mashed food pellets. Because of the poor health status of TBPQ64 rats at this end stage, and according to our animal health regulations, we had to kill all TBPQ64 rats after 10 months of age. Therefore, an analysis of lifespan was not possible, but considering the severe phenotype observed, it can be assumed that TBPQ64 rats have a decreased survival.

Motor deficits and increased anxiety in SCA17 rats

To assess progression of disease severity in TBPQ64 rats over time, we first repeatedly applied a modified ataxia score test (Guyenet et al., 2010), which has been successfully used in mouse models of cerebellar ataxia type 7. As expected, with increasing age the ataxia score increased significantly in SCA17 rats, reflecting a progression of symptoms (Fig. 3*A*; genotype by age, $F_{(4,68)} = 19.96$, $p < 0.0001$; genotype, $F_{(1,68)} = 40.55$, $p < 0.0001$). Already at the age of 5 weeks, TBPQ64 animals had a higher ataxia score than control animals; however, this difference became significant starting from the age of 5 months (Fig. 3*A*). Notably, during testing we observed that phenotypic TBPQ64 rats were not able to descend properly from a small beam into their home cage, but rather "fell" onto their head into the cage. To further analyze this apparent motor coordination and balance impairment, we performed rotarod and the beam-walking tests. Repeated-measures ANOVA revealed a significant main effect of genotype ($F_{(1,51)} = 5.53$, $p = 0.031$). Unexpectedly, by subsequent *post hoc* analysis with Bonferroni tests, we found no significant differences in the latency to fall between TBPQ64 and wild-type animals until the age of 8 months regarding the single time points (Fig. 3*B*). However, in the beam-walking test, transgenic animals showed significant difficulties in traversing the beams of different shapes and width (square beam with 3 cm cross section, genotype by age, $F_{(3,51)} = 4.15$, $p < 0.01$; genotype, $F_{(1,51)} = 48.99$, $p < 0.0001$; round beam with 3.5 cm diameter, genotype by age, $F_{(3,51)} = 11.36$, $p < 0.0001$; genotype, $F_{(1,51)} = 34.66$, $p < 0.0001$). TBPQ64 rats slipped more often when traversing the beams compared to age-matched control animals (Fig. 3*C*,*D*). Interestingly, there was no significant difference in the latency to traverse the various beams between both genotypes (data not shown). It should be noted that because of the severe phenotype at the age

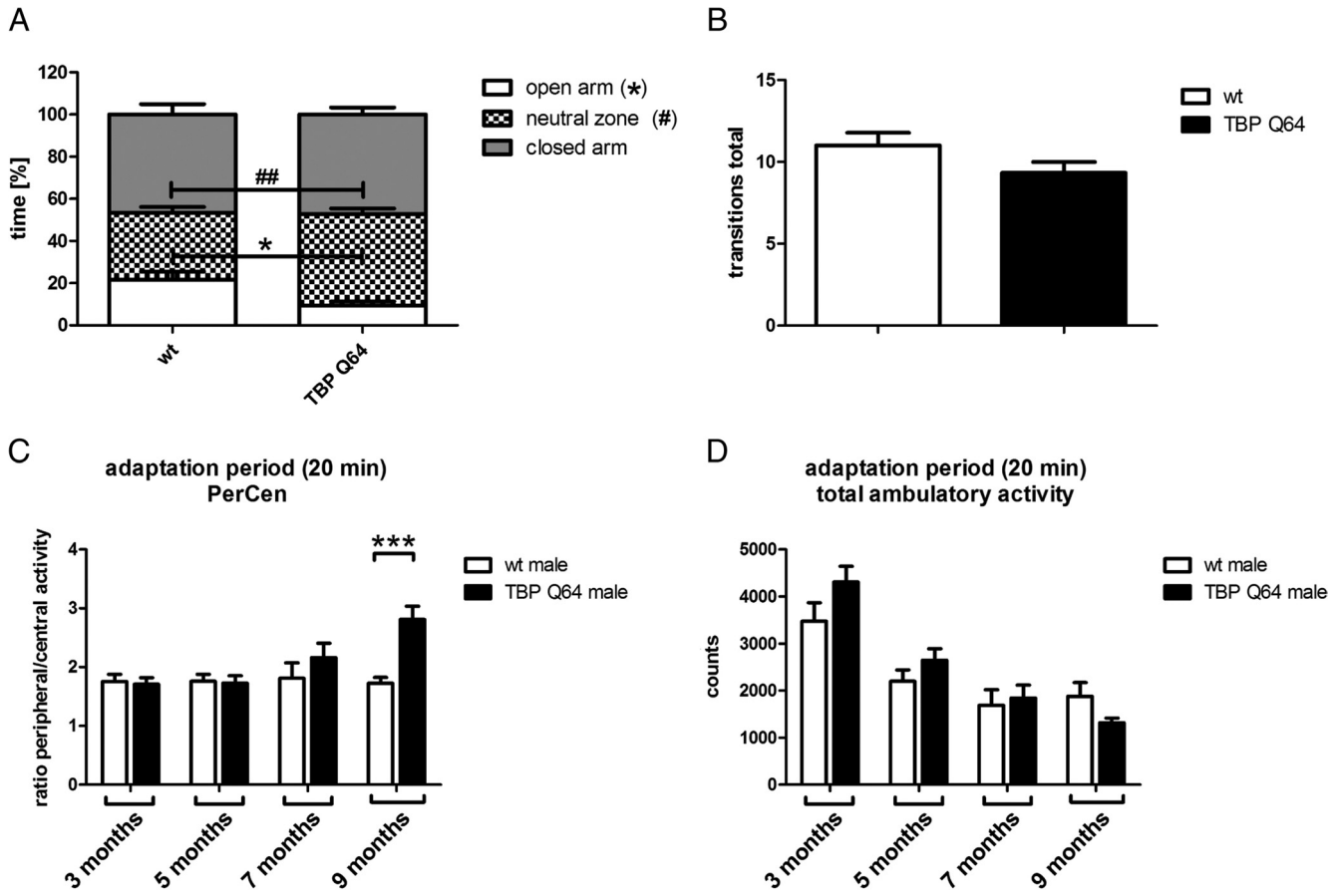

Figure 4. Measurements of anxiety-like behavior in SCA17 rats. ***A***, EPM performance. Male rats were tested at the age of 4 months [wild type (wt), $n = 17$; TBPQ64, $n = 15$] for 5 min on an EPM. Transgenic rats spent significantly less time on the open arm (white part of the columns) as well as in the middle zone, indicating an increased anxiety-like behavior in these animal than in controls. White columns represent the time spent on the open arm, checked columns represent time sent in the middle zone, and gray areas represent the time spent on the closed arm. $^{*}p < 0.05$; $^{\#\#}p < 0.01$; $^{***}p < 0.001$. ***B***, Total arm transitions on the EPM. There were no significant differences in the activity of transgenic and wild-type rats. ***C***, ***D***, Activity measurements during the adaptation period (first 20 min) of the PhenoMaster system. The periphery to center activity ratio (***C***) was significantly increased in old transgenic animals (9 months) compared to the controls, whereas no significant differences could be detected in the total ambulatory activity (***D***).

of 10 months, we could not perform these motor tests at this age.

Since psychiatric symptoms and behavioral symptoms are present in SCA17 patients, we assessed anxiety in the EPM test, which has been validated behaviorally and pharmacologically extensively (Pellow et al., 1985; Huang et al., 2012). Already at the age of 4 months, significant differences were found between TBPQ64 rats and their wild-type littermates (Fig. 4). Transgenic animals spent significantly less time on the open arms as well as significantly more time in the central zone than wild-type littermates, indicating that TBPQ64 rats have an increased anxiety (Fig. 4*A*). There were no differences in general activity between SCA17 rats and wild-type rats in the EPM test, as no significant differences in the total number of transitions into the various arms were observed (Fig. 4*B*). However, TBPQ64 rats showed significantly less transitions into the open arms (data not shown) and spent more time in the center area (neutral zone; Fig. 4*A*), supporting the notion that TBPQ64 rats are more anxious than wild-type littermates to enter the open arms. Furthermore, it was apparent that TBPQ64 rats had problems with keeping the balance as 20% of the transgenic animals fell from the open arms of the EPM, while this did not occur in the control group.

To provide further support of increased anxiety-related behavior in SCA17 rats, we analyzed the adaptation period (the first 20 min) in the PhenoMaster system, which is the time the animals need to adapt to the system or the new environment. The periphery to center ambulation ratio measurement is similar to the open-field test for anxiety in a novel environment. At the ages of 3 and 5 months, TBPQ64 rats and their wild-type littermates displayed the same ratio of peripheral to central activity (Fig. 4*C*). But starting at 7 months, TBPQ64 rats showed a higher ratio of periphery to center ambulation than controls, which reached significance at 9 months of age (Fig. 4*C*). This indicates an increased anxiety-like behavior in TBPQ64 rats and supports our findings in the EPM test. Regarding the total ambulatory activity in the adaptation period, we did not find significant differences (Fig. 4*D*).

Decreased activity in SCA17 rats

As SCA17 rats appeared to be less active, we evaluated the activity of TBPQ64 rats and their wild-type littermates in the PhenoMaster system that supplies quantitative measures. Animals were tested at 3, 5, 7, and 9 months of age. They were housed singly for 72 h in a home cage while rearing behavior and the total ambulatory activity was monitored continuously during these 72 h. Both transgenic and wild-type rats showed a pronounced dark/light cycle in their behavioral activities, with their main activity taking place during the dark phases. Exemplarily, data of the activity pattern are shown for 3 and 9 months of age, respectively (Fig. 5*A*,*B*). We observed a decreased rearing behavior in

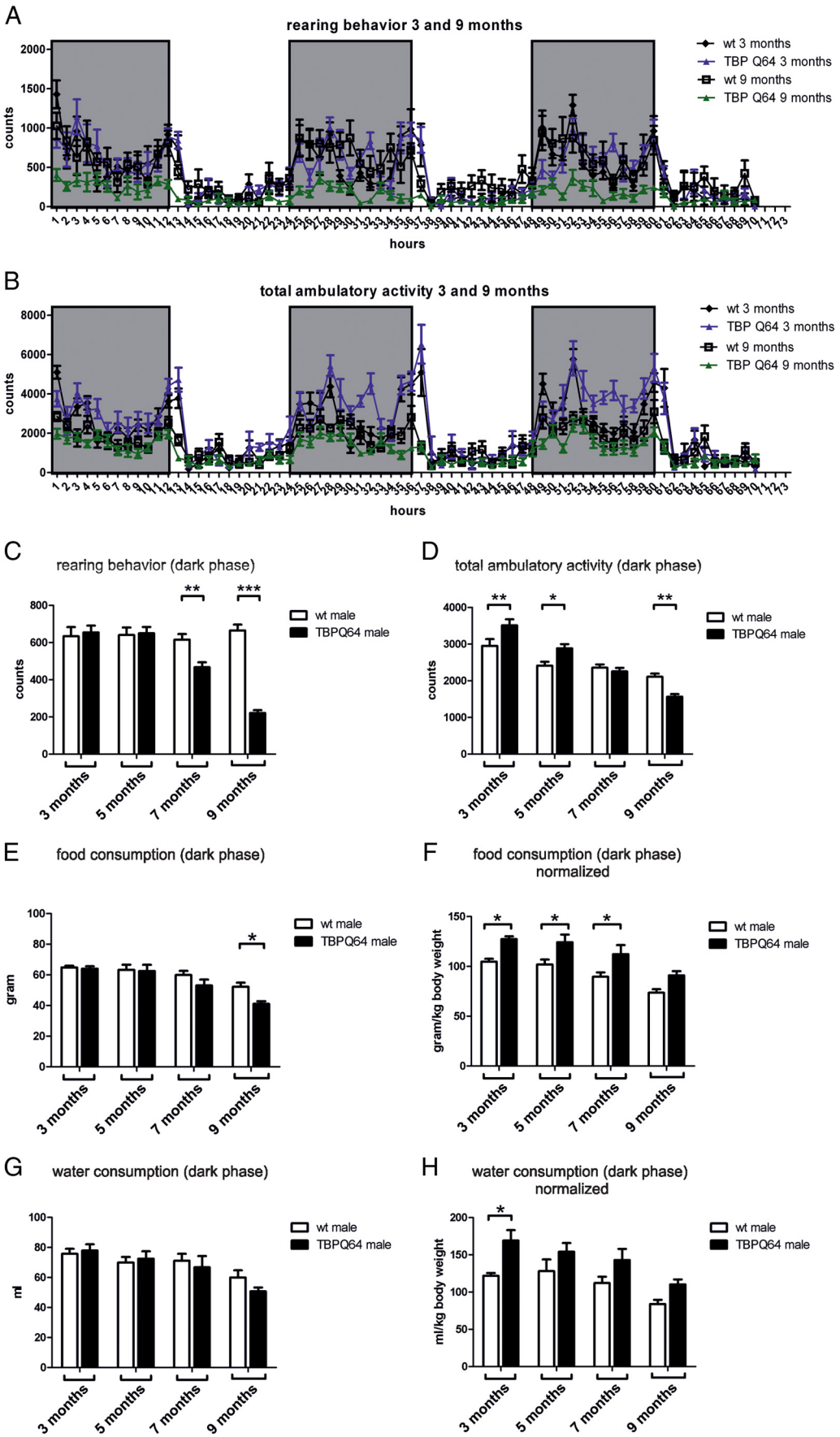

Figure 5. Activity in SCA17 rats decreases with age and progression of symptoms. ***A***, ***B***, The total ambulatory activity (***B***) and the rearing behavior (***A***) as measured in the PhenoMaster system are significantly decreased in male transgenic SCA17 rats at the age of 9 months (green triangle, $n = 9$) compared to 3-month-old animals (blue triangle) and age-matched (*Figure legend continues.*)

9-month-old transgenic animals when compared to controls of the same age and to 3-month-old TBPQ64 rats (Fig. 5*A*). Furthermore, 3-month-old TBPQ64 rats showed an increased total ambulatory activity in comparison to their wild-type littermates and to 9-month-old transgenic rats. The latter were less active than both age-matched controls and 3-month-old transgenic rats (Fig. 5*B*).

When analyzing the activity pattern, it was evident that differences between TBPQ64 rats and wild-type rats were pronounced in the dark cycle, the animals' active phase, so that subsequent analyses of all time points tested are restricted to the dark phase. Rearing behavior decreased in TBPQ64 rats with age (genotype by age, $F_{(3,280)} = 19.93$, $p < 0.0001$; genotype, $F_{(1,280)} = 33.70$, $p < 0.0001$), mirroring progression of symptoms. We found no differences between both genotypes at 3 and 5 months, but detected a significant decrease of rearing in 7- and 9-month-old TBPQ64 rats (Fig. 5*C*) compared to controls. Interestingly, ambulatory activity showed a biphasic profile as transgenic rats at the ages of 3 and 5 months were more active than control animals, whereas at 9 months of age the total ambulatory activity was significantly decreased in TBPQ64 rats compared to wild-type rats (Fig. 5*D*; genotype by age, $F_{(3,280)} = 9.349$, $p < 0.0001$; genotype, $F_{(1,280)} = 48.42$, $p < 0.0001$).

Moreover, we analyzed the feeding and drinking behavior of these rats (Fig. 5*E–H*). Graphs in Figure 5, *E* and *G*, shows absolute values, but as transgenic animals display such a low body weight at later stages, we also normalized the consumed food and liquid to the body weight of the animals (grams of food consumed per kilogram of body weight, or milliliter of liquid consumed per kilogram of body weight) in Figure 5, *F* and *H*. Despite their lower body weight, TBPQ64 rats had similar total food intake and water consumption until 7 months of age. Only at 9 months of age, when TBPQ64 rats are severely affected, was food intake significantly reduced in TBPQ64 rats compared to controls (Fig. 5*E*). When normalizing the food intake and water consumption to the body weight, we detected a significantly higher food intake at the ages of 3, 5, and 7 months in transgenic rats; at 9 months of age this increase in food intake did not reach significance (Fig. 5*F*; genotype by age, $F_{(3,48)} = 0.1154$, not significant; genotype, $F_{(1,48)} = 27.48$, $p < 0.0001$). Water consumption was also increased in transgenic rats (genotype, $F_{(1,48)} = 9.768$, $p < 0.01$), but the values reached significance only for the 3-month-old animals when applying the *post hoc* tests (Fig. 5*H*; genotype by age, $F_{(3,48)} = 0.5727$, not significant).

Immunohistochemistry and neurodegeneration in the cerebellum of SCA17 rats and human SCA17 brain

At the ages of 3 and 10 months, we investigated the cerebellar cortex by TuJ immunohistochemistry (Fig. 6*A–D*) and analyzed cellular and subcellular localization of TBP in TBPQ64 rats (Figs. 6*E–H*, 7*A–I*), where it is most predominantly expressed (Fig. 1*B*,*C*).

TuJ-1 staining lacked in the stellate and basket cells among the dendrites of degenerating Purkinje cells (PCs) in both young and 10-month-old TBPQ64 rats (Fig. 6*B*,*D*), whereas wild-type animals showed normal branching of the PC dendrites (slightly varying according to the tilt of section) and regular staining of interneurons in the molecular layer (Fig. 6*A*,*C*). Strong TBP immunoreactivity was detected mainly in the granule cell layer and the interneurons of the molecular layer, and less expressed in the Purkinje cell nuclei of TBPQ64 rats (Fig. 6*F*,*H*). Some unspecific staining was also observed in age-matched wild-type rats (Fig. 6*E*,*G*). Staining with a myc antibody showed a similar distribution of myc-tagged mutant TBP (Fig. 6*J*) as observed with the 1C2 antibody (Fig. 6*F*,*H*), whereas the wild types displayed only very faint endogenous myc protein (Fig. 6*I*). Some of the abnormalities observed in the transgenic rats resembled

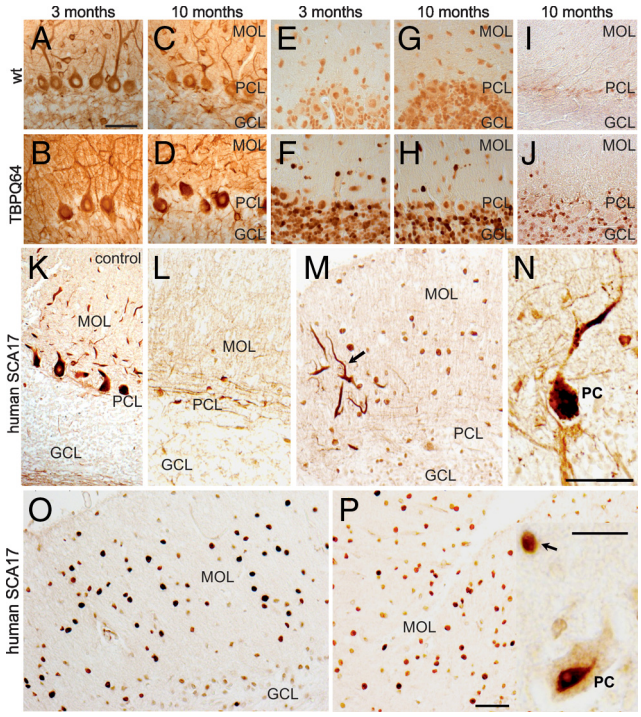

Figure 6. Cerebellar cortex in SCA17 rat and human SCA17 brain. ***A–J***, SCA17 rat. ***L–P***, Human SCA17. ***A–D***, Immunohistochemistry with monoclonal antibody TUJ-1 against class III-β-tubulin. ***E–H***, Immunohistochemistry with monoclonal antibody 1C2 against polyglutamine. ***I***, ***J***, Immunohistochemistry with a monoclonal antibody against myc. The class III-β-tubulin staining shows abnormalities in Purkinje cell bodies and dendrites (***B***, ***D***). At 3 months, the dendritic tree of SCA17 rats is still intact though reaction product in stellate and basket cells is absent (***B***). At 10 months, the dendritic tree is impoverished (***D***). The anti-polyglutamine antibody revealed specific neuronal immunohistochemistry only in the transgenic animals (***F***, ***H***) but not in the cerebellar cortex of the wild-type (wt) animals (***E***, ***G***). Inclusion bodies were most abundant in the granule cell layer (GCL), though a few were also present in the molecular layer (MOL). PCL, Purkinje cell layer. Myc staining confirmed the distribution of mutant TBP (***J***), as seen with 1C2, whereas the WT only displayed endogenous myc protein (***I***). ***L–P***, Human SCA-17 (Q55/Q38). ***K***, Normal human control cerebellum. ***K–N***, Immunohistochemistry with TUJ-1 against class III-β-tubulin. The cerebellar cortex of the SCA17 patient (***L–N***) shows Purkinje cell loss (***L***), a few distorted dendrites (***M***), and an impoverished dendritic tree (***N***). For comparison, the control section (***K***) displays intact Purkinje cells. ***O***, Polyglutamine staining with 1C2. ***P***, Inset, Immunohistochemistry with an antibody to TATA-binding protein; the MOL in ***M*** displays polyglutamine-positive nuclear inclusions that resemble the status in SCA17 rats (***F***, ***H***). Anti-TATA-binding protein shows a similar result (***P***). Only a few Purkinje cells show TATA-binding protein reaction product (***P***, inset). Sale bars: (in ***A***) ***A–J***, 50 μm; (in ***P***) ***K–M***, ***O***, ***P***, 50 μm; ***N***, inset in ***P***, 20 μm.

←

(*Figure legend continued.*) controls (black circles, 3 months; black squares, 9 months; $n = 9$). Gray rectangles represent the dark phase. ***C***, ***D***, Significant decrease of rearing behavior (***C***) and total ambulatory activity (***D***) over time in the dark phase in transgenic rats ($n = 9$; black column). ***E–H***, Absolute food (***E***) and water consumption (***G***) compared to normalized values (food, ***E***, ***F***; water consumption, ***G***, ***H***) during the dark phase. Measurements of food and water uptake at 3 and 5 months of age do not show significant differences, whereas at 7 and 9 months, transgenic rats (black columns) consumed less food and water than control animals (***E***, ***G***, white columns). Taking into account that TBPQ64 rats, especially at later time points, show less body weight, normalization according to the weight was necessary (***F***, ***H***). These graphs show that control animals ate and drank less compared to transgenic animals. At the age of 3–7 months, there are significant differences in the food consumption (***F***), comparing wild-type animals (white columns) with age-matched TBP Q6 rats (black columns). wt, Wild type. $^{*}p < 0.05$; $^{**}p < 0.01$; $^{***}p < 0.001$.

the cerebellar lesions of a patient with SCA17. Immunostaining with TuJ-1 revealed severe loss of Purkinje cells and tortuosity of the remaining dendrites (Fig. 6*M*,*N*). Basket and stellate neurons in the molecular layer (Fig. 6*L*) lacked TuJ-1 immunoreactivity when compared with a healthy control (Fig. 6*K*). As already observed in the transgenic rat, TBP reaction product occurs in numerous interneurons of the molecular layer (Fig. 6*O*,*P*), a subset of granule cells but only in very few Purkinje cell nuclei (Fig. 6*P*, inset).

Electron microscopy confirms neurodegeneration and nuclear TBP immunoreactivity in the cerebellum of SCA17 rats

Semithin and ultrathin sections showed specific nuclear TBP immunoreactivity in a subpopulation of granule cells, in numerous stellate, and some Purkinje cells in heterozygous TBPQ64 rat cerebellar cortex (Fig. 7). Immunopositive granule cells were often localized in groups between unstained cells. The nuclear TBP reactivity was varying in expression (Fig. 7*A*,*B*,*H*); several positive granule cell nuclei exhibited dysmorphic features (Fig. 7*H*). Some Purkinje cells showed tiny immunopositive intranuclear spots (Fig. 7*A*), clearly detected by electron microscopy (Fig. 7*D*).

Dark Purkinje cells were frequently observed (Fig. 7*A*) when compared with the cerebellar cortex of wild-type littermates (Fig. 7*C*), indicating Purkinje cell degeneration. The shrunken dark cytoplasm was often surrounded by degenerated basket fibers as detected electron microscopically (Fig. 7*E*). Dark Purkinje cell dendrites with irregular contours were also abundant in the molecular layer (Fig. 7*A*,*F*) confirming the distorted dendrites observed light microscopically (Fig. 6*D*). TBP-immunopositive nuclei of stellate cells (Fig. 7*B*,*G*) also reflected the results in the TBPQ64 rats (Fig. 6*F*,*H*) and human SCA17 brains (Fig. 6*O*,*P*). In the granule cell layer, numerous degenerated structures with dense lysosomal inclusions were observed, often associated with the glomerula (Fig. 7*I*).

Calbindin immunoreactivity was found to be reduced in Purkinje cell somata of TBPQ64 rats (Fig. 7*J*) when compared with wild-type littermates (Fig. 7*L*). The dendritic trees appeared distorted, also confirming the observations by the TuJ-1 antibody (Fig. 6*B*,*D*). Electron microscopically, calbindin-immunopositive Purkinje cell dendrites and spines were detected in the molecular layer neighbored to strongly degenerated dark dendrites lacking immunoreactivity (Fig. 7*K*).

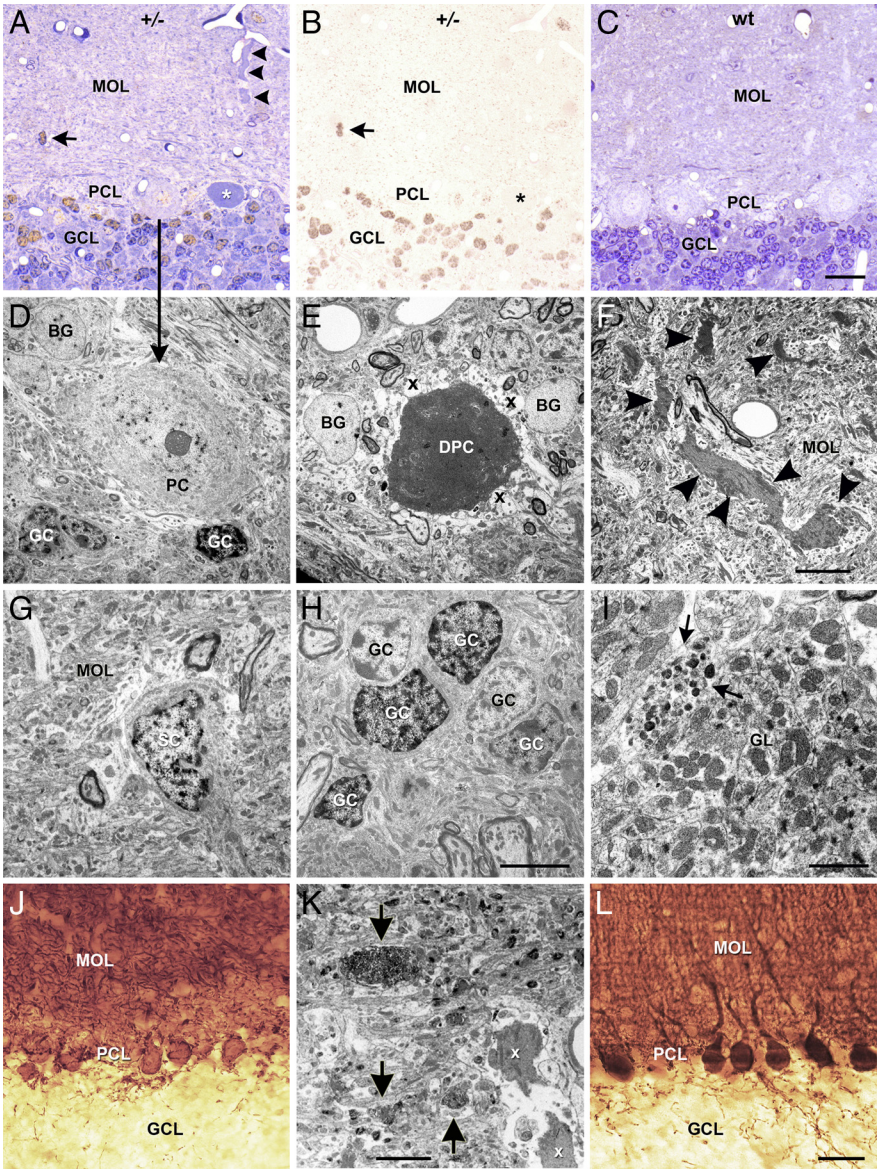

Figure 7. ***A–L***, Neurodegeneration, TBP (***A–I***), and calbindin (***J–L***) immunoreactivity in the cerebellum of 9-month-old male TBPQ64 (+/−) rats. Semithin (***A–C***) and ultrathin sections (***D–I***) showing nuclear TBP immunoreactivity and neurodegeneration, calbindin-immunostained vibratome slices (***J***, ***L***), and ultrathin sections (***K***) with Purkinje cell affection. ***A***, Semithin section counterstained with Toluidine blue shows TBP-immunopositive (light brown) and negative (blue) cells distributed in the granule cell layer (GCL) of a TBPQ64 rat, also detected in the adjacent section without counterstaining (***B***). The Purkinje cell (asterisks in ***A***, ***B***) undergoing dark cell degeneration sends a dark dendrite (***A***, arrowheads) toward the molecular layer (MOL). The adjacent Purkinje cell without signs of dark cell degeneration displays faint (light brown) nuclear TBP reaction product. The nucleus of a stellate cell (SC; ***A***, ***B***, arrows) in the MOL is also TBP immunopositive. ***C***, Semithin section shows normal cerebellar cortex of a wild-type (wt) littermate rat. ***D***, Electron microscopy of the Purkinje cell displays small TBP-positive spots in the nucleus, not observed in the cytoplasm. Note adjacent granule cells (GCs), where the TBP immunoreaction product is distributed in the caryoplasm. ***E***, The dark Purkinje cell (DPC) with nuclear and cytoplasmic condensation is surrounded by degenerating light appearing perisomatic basket fibers (x). ***F***, Numerous dark Purkinje cell dendrites with ruffled appearance are detected in the MOL (arrowheads). ***G***, Electron microscopy shows TBP immunoreactivity distributed in the caryoplasm of the SC and GC (***H***), the latter also between light appearing immunonegative GC nuclei. ***I***, A degenerating structure with multiple electron dense inclusions (arrows) is localized within a glomerulum (GL). ***J***, Calbindin-immunostained vibratome section shows faint and partly shrunken PCs and distorted dendritic trees in the MOL of a TBPQ64 rat. ***K***, Ultrathin section of the MOL reveals immunopositive PC dendrites (arrows) adjacent to dark dendrites (x), some of which are associated with light appearing climbing fibers with signs of degeneration. ***L***, The WT littermate displays normal Calbindin staining of PC somata and dendrites. BG, Bergmann glia; PCL, Purkinje cell layer. Scale bars: (in ***C***) ***A–C***, 20 μm; (in ***F***) ***D–F***, 5 μm; (in ***H***) ***G***, ***H***, 5 μm; ***I***, 1 μm; ***K***, 5 μm; (in ***L***) ***J***, ***L***, 20 μm.

PET and DTI imaging in SCA17 rats

Dynamic PET scans showed a specific uptake of the D_2 receptor antagonist [^{11}C]raclopride in the striatum of wild-type and transgenic rats at 10 months of age (Fig. 8*A*, *B*, black circles). This

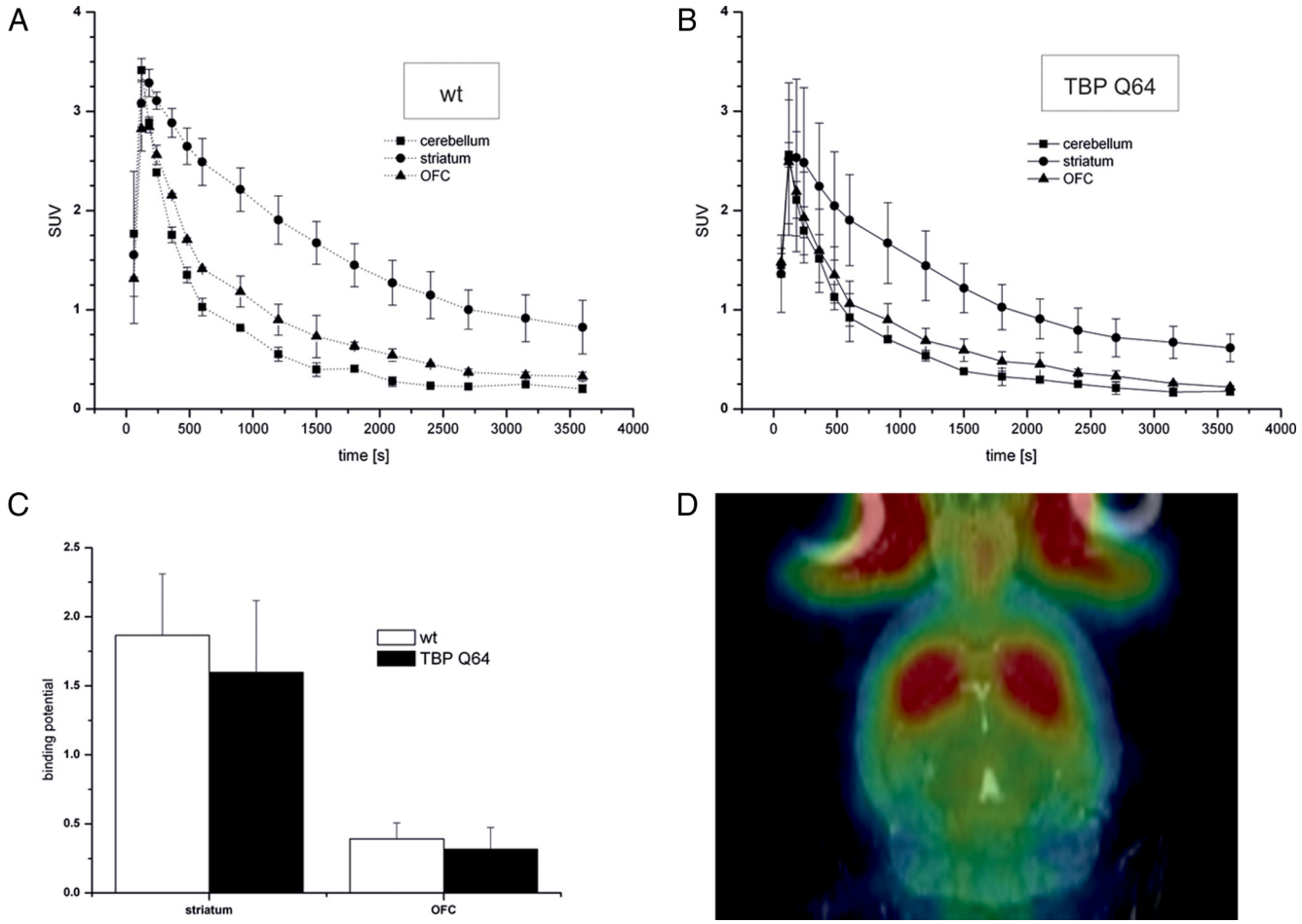

Figure 8. PET-imaging in SCA17 rats. ***A***, ***B***, [^{11}C]raclopride uptake measured as standard uptake volume (SUV) of different brain areas. PET time activity curves (TACs) of target (OFC and striatum) and reference regions (cerebellum) are plotted for the control (***A***) and TBPQ64 rats (***B***). ***C***, Corresponding binding potential (BP_{ND}) values are shown for the OFC and the striatum. In ***A*** and ***B***, error bars represent the SD of each time frame, and the mean BP_{ND} in ***C***. There is no significant difference in BP_{ND} between transgenic and control rats. ***D***, A representative image of a coregistered PET MRT image is shown.

effect did not occur in the cerebellum or the OFC. Interestingly, there is only a trend toward significance in the striatal TACs between wild-type and transgenic rats ($p = 0.061$). Also, the binding potential, while indicating a difference between transgenic and wild-type rats, did not reach significance (Fig. 8*C*). Because of the increased perfusion in the cerebellum in the first 15 min in transgenic compared to wild-type rats, we acquired ADC maps of these rats (Fig. 9). We observed that the cerebellar diffusion in SCA17 rats is significantly higher than in wild-type controls ($p < 0.001$). This strong effect only occurs in the cerebellum, while in dorsal striatum only a small trend toward significance could be shown ($p = 0.067$; Fig. 9*D*).

FA comparisons of the SCA17 and wild-type groups showed a clear tendency for lower FA values in the external capsule in the transgenic group, reaching statistical significance ($p = 0.032$; Fig. 9*C*). No significant difference in the dorsal striatum or the SN was observed ($p > 0.3$, not significant).

To investigate whether these changes in diffusion tension imaging occurred at an earlier age, we also examined a separate cohort of rats at the age of 5 months. However, at this age no significant differences in FA and ADC values in any of the investigated brain regions were found between TBPQ64 rats and wild-type rats (Fig. 9*A*,*B*).

Discussion

We generated and characterized the first transgenic rat model for spinocerebellar ataxia type 17. TBPQ64 rats showed characteristic phenotypic abnormalities and neuropathological changes similar to findings in human SCA17 patients. While some of these changes are well recapitulated in existing mouse models for SCA17, we provide evidence that crucial characteristics of SCA17 are better mirrored in our transgenic rats and that they represent a valuable tool to pursue experimentation and therapeutic approaches, currently difficult or impossible to perform with existing SCA17 transgenic mice.

A progressive loss of body weight was observed starting at 5 months of age leading to severe cachexia, so that all transgenic rats had to be killed after 10 months of age. This striking body weight loss is in line with findings in a transgenic mouse model for SCA17, although a peculiar increase of body weight preceded weight loss in these transgenic mice (Friedman et al., 2007). For another transgenic mouse model of SCA17 with a severe phenotype, no changes in body weight were described (Chang et al., 2011). In this regard, our transgenic rat model resembles more closely the human condition (Koide et al., 1999; Zühlke et al., 2001; Rolfs et al., 2003; Mariotti et al., 2007), e.g., reduced body weight (Koide et al., 1999). A similar body weight phenotype was observed in the only existing knock-in mouse model for SCA17 (Huang et al., 2011). However, as with other knock-in models of polyQ diseases (Wheeler et al., 2000; Lin et al., 2001; Menalled et al., 2002), these have a milder phenotype and do not die prematurely. This milder phenotype would require the use of large numbers of animals and a longer period of testing to determine a

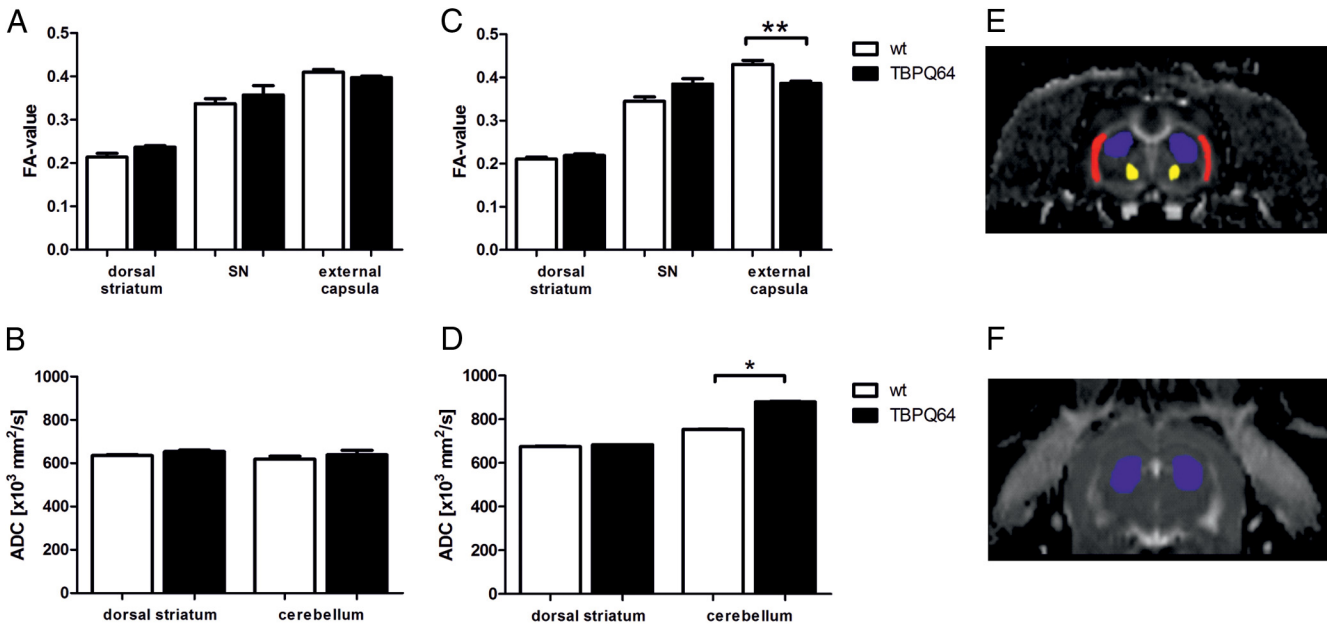

Figure 9. DTI in SCA17 rats. ***A***, ***C***, FA values measured in the dorsal striatum, the SN, and the external capsule in 5-month-old (***A***) and 10-month-old (***C***) rats. Transgenic rats are shown in black, whereas FA values of wild-type littermates are shown in white columns. Error bars represent the SD of FA values for each brain area. Significant effects between groups are indicated with asterisks (**$p < 0.01$). ***B***, ***D***, ADC values measured in the cerebellum and the striatum of wild-type (white columns) and transgenic (black columns) rats at the ages of 5 months (***B***) and 10 months (***D***). Error bars represent the SEM ADC values for each brain area. Significant effects between groups were illustrated with black stars (*$p < 0.05$). ***E***, ***F***, A representative diffusion tensor image (***E***) and a representative ADC map (***F***) are shown. The analyzed VOIs (***E***) according to the abovementioned coordinates are color coded (blue, dorsal striatum; yellow, ventral striatum; red, external capsule).

significant effect of an intervention, possibly decreasing the feasibility of such studies.

We also demonstrated that weight loss cannot be contributed to a lower food intake in TBPQ64 rats (Fig. 5*E*). In fact, when normalizing to the body weight, TBPQ64 rats even had a significantly higher food intake (Fig. 5*F*), indicating that increased metabolism might underlie the weight loss. Comparable observations have been made in HD mice where it was shown that weight loss in R6/2 mice is associated with elevated oxygen consumption and abnormalities in several weight-regulation factors (van der Burg et al., 2008) as well as mitochondrial dysfunction and impaired energy metabolism (Grünewald and Beal, 1999; Weydt et al., 2006). Further studies will be required to investigate whether the weight loss in SCA17 and HD are based on the same pathomechanisms.

Interestingly, besides severe ataxia and motor coordination problems (Fig. 3), we observed a biphasic activity profile in SCA17 rats with hyperkinesia in early stages of the disease progressing to bradykinesia at later stages (Fig. 5*D*). This is in agreement with findings in HD rodent models (Slow et al., 2003; André et al., 2011) and has been argued to reflect hyperkinetic symptoms such as chorea, and bradykinetic symptoms (e.g., dystonia or rigidity) at different stages of the disease (Slow et al., 2003). The prodromal hyperactive phase has not been described in the SCA17 mouse models so far (Chang et al., 2011; Huang et al., 2011), which might be due to the higher CAG repeat sizes in these models compared to our TBPQ64 rats. Higher CAG repeat sizes correlate with an earlier onset of disease and an increased severity of symptoms resulting in a different phenotype (Fujigasaki et al., 2001; Nakamura et al., 2001; Zühlke et al., 2001; Rolfs et al., 2003). In HD, for example, repeat sizes of >60 CAGs will lead to juvenile HD with bradykinesia and dystonia as predominant motor symptoms rather than chorea (Siesling et al., 1997; Squitieri et al., 2006; Quarrell et al., 2009). Animal models such as our TBPQ64 rats, which exhibit a biphasic activity profile, will be of great value to investigate the contribution of the indirect pathway to the development of hyperkinetic symptoms such as chorea as it has been shown in an HD patient (Starr et al., 2008), and to test therapeutics targeted to this pathway. Furthermore, the larger size of rats facilitates greatly the use of *in vivo* electrophysiology, which will be essential to understand how the neuronal circuitry is affected and how compounds such as phospodiesterase 10 inhibitors could restore the function of indirect pathway neurons not only in HD but also in SCA17 (Threlfell et al., 2009; Beaumont, 2012).

Unlike the other spinocerebellar ataxias, SCA17 is not only characterized by progressive cerebellar ataxia, but also a broad spectrum of other neuropsychiatric signs (Zühlke et al., 2001; Mariotti et al., 2007). Mouse models are in general limited for studying these functional and behavioral measurements (Tecott and Nestler, 2004; Rodriguiz and Wetsel, 2006), especially since most standard test designs were originally developed and validated for rats. Whether they can be transferred to mice by mere downsizing of the test systems is unclear. Therefore, TBPQ64 rats are a valuable resource to study nonmotor abnormalities in SCA17. Indeed, we demonstrated increased anxiety-like behavior for the first time in a rodent model of SCA17 paralleling the human condition (Zühlke et al., 2001; Mariotti et al., 2007). This is especially interesting as several anxiolytic drugs are available, which have been validated in rats using the elevated plus maze for more than two decades (reviewed in File, 1990). Whether cognitive changes are also present in TBPQ64 rats has not been evaluated in the current study but testing will be readily feasible in this rat model in future studies.

Neuropathologically, the severe phenotype of SCA17 rats was associated with neuronal loss, particularly in the cerebellum. Degeneration of Purkinje cells, basket cells, and stellate neurons; changes and degenerations in the morphology of the Purkinje cell

dendrites; axonal torpedos; and TBP-positive immunoreactivity of stellate and basket cells in the molecular layer were readily found by light and electron microscopy (Fig. 6; 7), consistent with findings in human SCA17 patients (Fig. 6) (Rolfs et al., 2003). Interestingly, we also observed numerous TBP-positive granule cells adjacent to immunonegative cells, which was not found to this extent in the human SCA17 patients investigated here. However, there is a report of nuclear TBP reactivity in granule cell nuclei in SCA17 human patients (Fujigasaki et al., 2001). The abundant expression of mutant TBP in granule cells of the TBPQ64 rat may be due to the prion promoter construct that we used and in agreement with the known expression pattern of the transgene expression driven by this promoter (Borchelt et al., 1996; Schilling et al., 1999a,b; Garden et al., 2002). Together, the neuropathological changes detected in the TBPQ64 rats recapitulate many characteristics of human SCA17 and extend findings in SCA17 mouse models (Friedman et al., 2007; Chang et al., 2011; Huang et al., 2011), especially in regard to changes in dendrite morphology.

To take advantage of the larger brain size of rats compared to mice, we performed *in vivo* PET and DTI imaging to detect a potential biomarker for SCA17. Previous PET data with the dopamine 2 receptor antagonist raclopride in SCA17 patients showed loss of postsynaptic D_2 receptors in the caudate nucleus (Brockmann et al., 2012). In our TBPQ64 rats, a decreased binding potential of the D_2 receptor antagonist [^{11}C]raclopride was found in the caudate–putamen, consistent with the human data, although this difference did not reach significance. This may be due to the low expression of mutant TBP in this brain region in the SCA17 rats, and maybe attributed to the use of the Prp promoter to drive transgene expression.

Since the D_2 receptor is expressed only at low levels in the cerebellum (Farde et al., 1985), the most affected brain region in the TBPQ64 rats, we applied DTI, which allows the observation of gray and white matter changes over time. In HD patients, DTI has also been shown to allow detection of altered tissue integrity in both preclinical and clinical stages of HD (Mascalchi et al., 2004; Reading et al., 2005; Rosas et al., 2006, 2010; Seppi et al., 2006; Bohanna et al., 2008; Klöppel et al., 2008; Douaud et al., 2009; Della Nave et al., 2010; Mandelli et al., 2010; Sritharan et al., 2010). DTI has also been successfully applied in an inducible rat model of HD (Van Camp et al., 2012) and in one of the transgenic rat models of HD (Antonsen et al., 2012; Blockx et al., 2012), as well as in other rodent disease models (Song et al., 2004; Boska et al., 2007; Lope-Piedrafita et al., 2008; Van Camp et al., 2009; Grundmann et al., 2012). DTI thus appears as a promising tool for monitoring neuropathology in transgenic SCA17 rats. In the TBPQ64 rats we detected a significant increase in cerebellar diffusion (higher ADC values) indicating cell death, which is in good agreement with our neuropathological findings (loss of basket and stellate neurons in the molecular layer, dark cell degeneration of PCs). Furthermore, we found a significant decrease of FA values in the external capsule, although no significant difference in the dorsal striatum, the ventral striatum, or the substantia nigra could be observed. The significantly lower FA value in the external capsule could hint to a degeneration of the fiber bundles that project to the dopaminergic neurons of the striatum. Consistent with this we had observed fiber degeneration in the striatum of some SCA17 rats (data not shown). Our results confirm that DTI measures are potentially useful correlates of neuropathological changes in these transgenic rats and raise hope that DTI imaging could provide a biomarker for SCA17 patients, which has not been pursued so far.

References

André M, Cepeda C, Fisher YE, Huynh M, Bardakjian N, Singh S, Yang XW, Levine MS (2011) Differential electrophysiological changes in striatal output neurons in Huntington's disease. J Neurosci 31:1170–1182. CrossRef Medline

Antonsen BT, Jiang Y, Veraart J, Qu H, Nguyen HP, Sijbers J, Von Hörsten S, Johnson GA, Leergaard TB (2012) Altered diffusion tensor imaging measurements in aged transgenic Huntington disease rats. Brain Struct Funct. Advance online publication. Retrieved July 27, 2012. CrossRef Medline

Beaumont V (2012) cGMP-hydrolyzing PDEs are therapeutic targets for Huntington's disease. PLoS One 7:e44498. CrossRef Medline

Bichelmeier U, Schmidt T, Hübener J, Boy J, Rüttiger L, Häbig K, Poths S, Bonin M, Knipper M, Schmidt WJ, Wilbertz J, Wolburg H, Laccone F, Riess O (2007) Nuclear localization of ataxin-3 is required for the manifestation of symptoms in SCA3: *in vivo* evidence. J Neurosci 27:7418–7428. CrossRef Medline

Blockx I, Verhoye M, Van Audekerke J, Bergwerf I, Kane JX, Delgado Y Palacios R, Veraart J, Jeurissen B, Raber K, Von Hörsten S, Ponsaerts P, Sijbers J, Leergaard TB, Van der Linden A (2012) Identification and characterization of Huntington related pathology: an *in vivo* DKI imaging study. Neuroimage 63:653–662. CrossRef Medline

Bohanna I, Georgiou-Karistianis N, Hannan AJ, Egan GF (2008) Magnetic resonance imaging as an approach towards identifying neuropathological biomarkers for Huntington's disease. Brain Res Rev 58:209–225. CrossRef Medline

Borchelt DR, Davis J, Fischer M, Lee MK, Slunt HH, Ratovitsky T, Regard J, Copeland NG, Jenkins NA, Sisodia SS, Price DL (1996) A vector for expressing foreign genes in the brains and hearts of transgenic mice. Genet Anal 13:159–163. CrossRef Medline

Boska MD, Hasan KM, Kibuule D, Banerjee R, McIntyre E, Nelson JA, Hahn T, Gendelman HE, Mosley RL (2007) Quantitative diffusion tensor imaging detects dopaminergic neuronal degeneration in a murine model of Parkinson's disease. Neurobiol Dis 26:590–596. CrossRef Medline

Boy J, Schmidt T, Wolburg H, Mack A, Nuber S, Böttcher M, Schmitt I, Holzmann C, Zimmermann F, Servadio A, Riess O (2009) Reversibility of symptoms in a conditional mouse model of spinocerebellar ataxia type 3. Hum Mol Genet 18:4282–4295. CrossRef Medline

Brockmann K, Reimold M, Globas C, Hauser TK, Walter U, Machulla HJ, Rolfs A, Schöls L (2012) PET and MRI reveal early evidence of neurodegeneration in spinocerebellar ataxia type 17. J Nuclear Med 53:1074–1080. CrossRef

Burley SK, Roeder RG (1996) Biochemistry and structural biology of transcription factor IID (TFIID). Annu Rev Biochem 65:769–799. CrossRef Medline

Casteels C, Vandeputte C, Rangarajan JR, Dresselaers T, Riess O, Bormans G, Maes F, Himmelreich U, Nguyen H, Van Laere K (2011) Metabolic and type 1 cannabinoid receptor imaging of a transgenic rat model in the early phase of Huntington disease. Exp Neurol 229:440–449. CrossRef Medline

Chang YC, Lin CY, Hsu CM, Lin HC, Chen YH, Lee-Chen GJ, Su MT, Ro LS, Chen CM, Hsieh-Li HM (2011) Neuroprotective effects of granulocyte-colony stimulating factor in a novel transgenic mouse model of SCA17. J Neurochem 118:288–303. CrossRef Medline

Della Nave R, Ginestroni A, Tessa C, Giannelli M, Piacentini S, Filippi M, Mascalchi M (2010) Regional distribution and clinical correlates of white matter structural damage in Huntington disease: a tract-based spatial statistics study. AJNR Am journal Neuroradiol 31:1675–1681. CrossRef

Douaud G, Behrens TE, Poupon C, Cointepas Y, Jbabdi S, Gaura V, Golestani N, Krystkowiak P, Verny C, Damier P, Bachoud-Lévi AC, Hantraye P, Remy P (2009) *In vivo* evidence for the selective subcortical degeneration in Huntington's disease. Neuroimage 46:958–966. CrossRef Medline

Farde L, Ehrin E, Eriksson L, Greitz T, Hall H, Hedström CG, Litton JE, Sedvall G (1985) Substituted benzamides as ligands for visualization of dopamine receptor binding in the human brain by positron emission tomography. Proc Natl Acad Sci U S A 82:3863–3867. CrossRef Medline

File SE (1990) New strategies in the search for anxiolytics. Drug Des Deliv 5:195–201. Medline

Franklin K, Paxinos G (2001) Stereotactic brain atlas, Ed 2. San Diego: Academic.

Friedman MJ, Shah AG, Fang ZH, Ward EG, Warren ST, Li S, Li X-J (2007)

Polyglutamine domain modulates the TBP-TFIIB interaction: implications for its normal function and neurodegeneration. Nat Neurosci 10: 1519–1528. CrossRef Medline

Fujigasaki H, Martin JJ, De Deyn PP, Camuzat A, Deffond D, Stevanin G, Dermaut B, Van Broeckhoven C, Dürr A, Brice A (2001) CAG repeat expansion in the TATA box-binding protein gene causes autosomal dominant cerebellar ataxia. Brain 124:1939–1947. CrossRef Medline

Garden GA, Libby RT, Fu YH, Kinoshita Y, Huang J, Possin DE, Smith AC, Martinez RA, Fine GC, Grote SK, Ware CB, Einum DD, Morrison RS, Ptacek LJ, Sopher BL, La Spada AR (2002) Polyglutamine-expanded ataxin-7 promotes non-cell-autonomous Purkinje cell degeneration and displays proteolytic cleavage in ataxic transgenic mice. J Neurosci 22: 4897–4905. Medline

Grundmann K, Glöckle N, Martella G, Sciamanna G, Hauser TK, Yu L, Castaneda S, Pichler B, Fehrenbacher B, Schaller M, Nuscher B, Haass C, Hettich J, Yue Z, Nguyen HP, Pisani A, Riess O, Ott T (2012) Generation of a novel rodent model for DYT1 dystonia. Neurobiol Dis 47:61–74. CrossRef Medline

Grünewald T, Beal MF (1999) Bioenergetics in Huntington's disease. Ann N Y Acad Sci 893:203–213. CrossRef

Guyenet SJ, Furrer SA, Damian VM, Baughan TD, La Spada AR, Garden GA (2010) A simple composite phenotype scoring system for evaluating mouse models of cerebellar ataxia. J Vis Exp 39:2–4. CrossRef Medline

Herrmann KH, Schmidt S, Kretz A, Haenold R, Krumbein I, Metzler M, Gaser C, Witte OW, Reichenbach JR (2012) Possibilities and limitations for high resolution small animal MRI on a clinical whole-body 3T scanner. MAGMA 25:233–244. CrossRef Medline

Huang HY, Lee HW, Chen SD, Shaw FZ (2012) Lamotrigine ameliorates seizures and psychiatric comorbidity in a rat model of spontaneous absence epilepsy. Epilepsia 53:2005–2014. CrossRef Medline

Huang S, Ling JJ, Yang S, Li XJ, Li S (2011) Neuronal expression of TATA box-binding protein containing expanded polyglutamine in knock-in mice reduces chaperone protein response by impairing the function of nuclear factor-Y transcription factor. Brain 134:1943–1958. CrossRef Medline

Klöppel S, Draganski B, Golding CV, Chu C, Nagy Z, Cook PA, Hicks SL, Kennard C, Alexander DC, Parker GJ, Tabrizi SJ, Frackowiak RS (2008) White matter connections reflect changes in voluntary-guided saccades in pre-symptomatic Huntington's disease. Brain 131:196–204. Medline

Koeppen AH, Morral JA, McComb RD, Feustel PJ (2011) The neuropathology of late-onset Friedreich's ataxia. Cerebellum 10:96–103. CrossRef Medline

Koide R, Kobayashi S, Shimohata T, Ikeuchi T, Maruyama M, Saito M, Yamada M, Takahashi H, Tsuji S (1999) A neurological disease caused by an expanded CAG trinucleotide repeat in the TATA-binding protein gene: a new polyglutamine disease? Hum Mol Genet 8:2047–2053. CrossRef Medline

Korenova M, Zilka N, Stozicka Z, Bugos O, Vanicky I, Novak M (2009) NeuroScale, the battery of behavioral tests with novel scoring system for phenotyping of transgenic rat model of tauopathy. J Neurosci Methods 177:108–114. CrossRef Medline

Kujpers M (1999) Report of the NIH rat model priority. Bethesda, MD: NIH.

Laccone F, Maiwald R, Bingemann S (1999) A fast polymerase chain reaction-mediated strategy for introducing repeat expansions into CAG-repeat containing genes. Hum Mutat 13:497–502. CrossRef Medline

Lin CH, Tallaksen-Greene S, Chien WM, Cearley JA, Jackson WS, Crouse AB, Ren S, Li XJ, Albin RL, Detloff PJ (2001) Neurological abnormalities in a knock-in mouse model of Huntington's disease. Hum Mol Genet 10:137–144. CrossRef Medline

Lope-Piedrafita S, Garcia-Martin ML, Galons JP, Gillies RJ, Trouard TP (2008) Longitudinal diffusion tensor imaging in a rat brain glioma model. NMR Biomed 21:799–808. CrossRef Medline

Maltecca F, Filla A, Castaldo I, Coppola G, Fragassi NA, Carella M, Bruni A, Cocozza S, Casari G, Servadio A, De Michele G (2003) Intergenerational instability and marked anticipation in SCA-17. Neurology 61:1441–1443. CrossRef Medline

Mandelli ML, Savoiardo M, Minati L, Mariotti C, Aquino D, Erbetta A, Genitrini S, Di Donato S, Bruzzone MG, Grisoli M (2010) Decreased diffusivity in the caudate nucleus of presymptomatic Huntington disease gene carriers: which explanation? Am J Neuroradiol 31:706–710. CrossRef Medline

Mariotti C, Alpini D, Fancellu R, Soliveri P, Grisoli M, Ravaglia S, Lovati C, Fetoni V, Giaccone G, Castucci A, Taroni F, Gellera C, Di Donato S (2007) Spinocerebellar ataxia type 17 (SCA17): oculomotor phenotype and clinical characterization of 15 Italian patients. J Neurol 254:1538–1546. CrossRef Medline

Mascalchi M, Lolli F, Nave R Della, Tessa C, Petralli R, Gavazzi C, Politi LS, Macucci M, Filippi M, Piacentini S (2004) Huntington disease: volumetric, diffusion-weighted, and magnetization transfer MR imaging of brain. Radiology 232:867–873. Medline

Menalled LB, Sison JD, Wu Y, Olivieri M, Li X, Li H, Zeitlin S (2002) Early motor dysfunction and striosomal distribution of huntingtin microaggregates in Huntington's disease knock-in mice. J Neurosci 22:8266–8276. Medline

Miller BR, Walker AG, Fowler SC, von Hörsten S, Riess O, Johnson MA, Rebec GV (2010) Dysregulation of coordinated neuronal firing patterns in striatum of freely behaving transgenic rats that model Huntington's disease. Neurobiol Dis 37:106–113. CrossRef Medline

Nakamura K, Jeong SY, Uchihara T, Anno M, Nagashima K, Nagashima T, Ikeda S, Tsuji S, Kanazawa I (2001) SCA17, a novel autosomal dominant cerebellar ataxia caused by an expanded polyglutamine in TATA-binding protein. Hum Mol Genet 10:1441–1448. CrossRef Medline

Ortiz AN, Osterhaus GL, Lauderdale K, Mahoney L, Fowler SC, von Hörsten S, Riess O, Johnson MA (2012) Motor function and dopamine release measurements in transgenic Huntington's disease model rats. Brain Res 1450:148–156. CrossRef Medline

Pellow S, Chopin P, File SE, Briley M (1985) Validation of open:closed arm entries in an elevated plus-maze as a measure of anxiety in the rat. J of neuroscience methods 14:149–167. CrossRef

Petrasch-Parwez E, Nguyen HP, Löbbecke-Schumacher M, Habbes HW, Wieczorek S, Riess O, Andres KH, Dermietzel R, Von Hörsten S (2007) Cellular and subcellular localization of Huntingtin [corrected] aggregates in the brain of a rat transgenic for Huntington disease. J Comp Neurol 501:716–730. CrossRef Medline

Quarrell OWJ, Brewer HM, Squitieri F, Barker RA, Nance MA LB (2009) Juvenile Huntington's disease and other trinucleotide repeat disorders. Oxford, UK: Oxford UP.

Rath A, Klein A, Papazoglou A, Pruszak J, Garciaa J, Krause M, Maciaczyk J, Dunnett SB, Nikkhah G (2012) Survival and functional restoration of human fetal ventral mesencephalon following transplantation in a rat model of Parkinson's disease. Cell Transplant. Advance online publication. Medline

Reading SA, Yassa MA, Bakker A, Dziorny AC, Gourley LM, Yallapragada V, Rosenblatt A, Margolis RL, Aylward EH, Brandt J, Mori S, van Zijl P, Bassett SS, Ross CA (2005) Regional white matter change in pre-symptomatic Huntington's disease: a diffusion tensor imaging study. Psychiatry Res 140:55–62. CrossRef Medline

Rehbinder C, Baneux P, Forbes D, van Herck H, Nicklas W, Rugaya Z, Winkler G (1996) FELASA recommendations for the health monitoring of mouse, rat, hamster, gerbil, guinea pig and rabbit experimental units. Report of the Federation of European Laboratory Animal Science Associations (FELASA) Working Group on Animal Health accepted by the. Lab Anim 30:193–208. CrossRef Medline

Ribeiro D, Goya RL, Ravindran G, Vuono R, Parish CL, Foldi C, Piroth T, Yang S, Parmar M, Nikkhah G, Hjerling-Leffler J, Lindvall O, Barker RA, Arenas E (2012) Efficient expansion and dopaminergic differentiation of human fetal ventral midbrain neural stem cells by midbrain morphogens. Neurobiol Dis 49C:118–127. CrossRef Medline

Riley BE, Orr HT (2006) Polyglutamine neurodegenerative diseases and regulation of transcription: assembling the puzzle. Genes Dev 20:2183–2192. CrossRef Medline

Rodriguiz RM, Wetsel WC (2006) Assessments of cognitive deficits in mutant mice. In: Animal models of cognitive impairment, Chap 12.

Rolfs A, Koeppen AH, Bauer I, Bauer P, Buhlmann S, Topka H, Schöls L, Riess O (2003) Clinical features and neuropathology of autosomal dominant spinocerebellar ataxia (SCA17). Ann Neurol 54:367–375. CrossRef Medline

Rosas HD, Tuch DS, Hevelone ND, Zaleta AK, Vangel M, Hersch SM, Salat DH (2006) Diffusion tensor imaging in presymptomatic and early Huntington's disease: selective white matter pathology and its relationship to clinical measures. Movement Dis 21:1317–1325. CrossRef Medline

Rosas HD, Lee SY, Bender AC, Zaleta AK, Vangel M, Yu P, Fischl B, Pappu V, Onorato C, Cha JH, Salat DH, Hersch SM (2010) Altered white matter

microstructure in the corpus callosum in Huntington's disease: implications for cortical "disconnection." Neuroimage 49:2995–3004. CrossRef

Schilling G, Becher MW, Sharp AH, Jinnah HA, Duan K, Kotzuk JA, Slunt HH, Ratovitski T, Cooper JK, Jenkins NA, Copeland NG, Price DL, Ross CA, Borchelt DR (1999a) Intranuclear inclusions and neuritic aggregates in transgenic mice expressing a mutant N-terminal fragment of huntingtin. Human molecular genetics 8:397–407. CrossRef Medline

Schilling G, Wood JD, Duan K, Slunt HH, Gonzales V, Yamada M, Cooper JK, Margolis RL, Jenkins NA, Copeland NG, Takahashi H, Tsuji S, Price DL, Borchelt DR, Ross CA (1999b) Nuclear accumulation of truncated atrophin-1 fragments in a transgenic mouse model of DRPLA. Neuron 24:275–286. CrossRef Medline

Seppi K, Schocke MF, Mair KJ, Esterhammer R, Weirich-Schwaiger H, Utermann B, Egger K, Brenneis C, Granata R, Boesch S, Poewe W, Wenning GK (2006) Diffusion-weighted imaging in Huntington's disease. Movement Dis 21:1043–1047. CrossRef Medline

Siesling S, Vegter-van der Vlis M, Roos RA (1997) Juvenile Huntington disease in the Netherlands. Pediatric Neurol 17:37–43. CrossRef

Slow EJ, van Raamsdonk J, Rogers D, Coleman SH, Graham RK, Deng Y, Oh R, Bissada N, Hossain SM, Yang Y, Li X, Simpson EM, Gutekunst C, Leavitt BR, Hayden MR (2003) Selective striatal neuronal loss in a YAC128 mouse model of Huntington disease. Hum Mol Genet 12:1555–1567. Medline

Song SK, Kim JH, Lin SJ, Brendza RP, Holtzman DM (2004) Diffusion tensor imaging detects age-dependent white matter changes in a transgenic mouse model with amyloid deposition. Neurobiol Dis 15:640–647. CrossRef Medline

Squitieri F, Frati L, Ciarmiello A, Lastoria S, Quarrell O (2006) Juvenile Huntington's disease: does a dosage-effect pathogenic mechanism differ from the classical adult disease? Mechanisms of ageing and development 127:208–212. CrossRef Medline

Sritharan A, Egan GF, Johnston L, Horne M, Bradshaw JL, Bohanna I, Asadi H, Cunnington R, Churchyard AJ, Chua P, Farrow M, Georgiou-Karistianis N (2010) A longitudinal diffusion tensor imaging study in symptomatic Huntington's disease. J Neurol Neurosurg Psychiatry 81: 257–262. CrossRef Medline

Starr PA, Kang GA, Heath S, Shimamoto S, Turner RS (2008) Pallidal neuronal discharge in Huntington's disease: support for selective loss of striatal cells originating the indirect pathway. Exp Neurol 211:227–233. CrossRef Medline

Tecott LH, Nestler EJ (2004) Neurobehavioral assessment in the information age. Nat Neurosci 7:462–466. CrossRef Medline

Threlfell S, Sammut S, Menniti FS, Schmidt CJ, West AR (2009) Inhibition of phosphodiesterase 10A increases the responsiveness of striatal projection neurons to cortical stimulation. J Pharmacol Exp Ther 328:785–795. CrossRef

Tomiuk J, Bachmann L, Bauer C, Rolfs A, Schöls L, Roos C, Zischler H, Schuler MM, Bruntner S, Riess O, Bauer P (2007) Repeat expansion in spinocerebellar ataxia type 17 alleles of the TATA-box binding protein gene: an evolutionary approach. Eur J Hum Genet 15:81–87. CrossRef Medline

Urbach YK, Bode FJ, Nguyen HP, Riess O, Hörsten S Von (2010) Rat Genomics (Anegon I, ed). Totowa, NJ: Humana.

Van Camp N, Blockx I, Verhoye M, Casteels C, Coun F, Leemans A, Sijbers J, Baekelandt V, Van Laere K, Van der Linden A (2009) Diffusion tensor imaging in a rat model of Parkinson's disease after lesioning of the nigrostriatal tract. NMR Biomed 22:697–706. CrossRef Medline

Van Camp N, Blockx I, Camón L, de Vera N, Verhoye M, Veraart J, Van Hecke W, Martínez E, Soria G, Sijbers J, Planas AM, Van der Linden A (2012) A complementary diffusion tensor imaging (DTI)-histological study in a model of Huntington's disease. Neurobiol Aging 33:945–959. CrossRef Medline

van der Burg JMM, Bacos K, Wood NI, Lindqvist A, Wierup N, Woodman B, Wamsteeker JI, Smith R, Deierborg T, Kuhar MJ, Bates GP, Mulder H, Erlanson-Albertsson C, Morton AJ, Brundin P, Petersén A, Björkqvist M (2008) Increased metabolism in the R6/2 mouse model of Huntington's disease. Neurobiol Dis 29:41–51. CrossRef Medline

Weydt P, Pineda VV, Torrence AE, Libby RT, Satterfield TF, Lazarowski ER, Gilbert ML, Morton GJ, Bammler TK, Strand AD, Cui L, Beyer RP, Easley CN, Smith AC, Krainc D, Luquet S, Sweet IR, Schwartz MW, La Spada AR (2006) Thermoregulatory and metabolic defects in Huntington's disease transgenic mice implicate PGC-1alpha in Huntington's disease neurodegeneration. Cell Metab 4:349–362. CrossRef Medline

Wheeler VC, White JK, Gutekunst C, Vrbanac V, Weaver M, Li X, Li S, Yi H, Vonsattel J, Gusella JF, Hersch S, Auerbach W, Joyner AL, Macdonald ME (2000) Long glutamine tracts cause nuclear localization of a novel form of huntingtin in medium spiny striatal neurons in Hdh Q92 and Hdh Q111 knock-in mice. Hum Mol Genet 9:503–514.

Yu-Taeger L, Petrasch-Parwez E, Osmand A, Redensek A, Metzger S, Clemens LE, Park L, Howland D, Calaminus C, Gu X, Pichler B, Yang XW, Riess O NH (2012) A novel BACHD transgenic rat exhibits characteristic neuropathological features of Huntington's disease. J Neurosci 32: 15426–15438. CrossRef Medline

Zoghbi HY, Orr HT (2000) Glutamine repeats and neurodegeneration. Annu Rev Neurosci 23:217–247. CrossRef Medline

Zühlke C, Hellenbroich Y, Dalski A, Kononowa N, Hagenah J, Vieregge P, Riess O, Klein C, Schwinger E (2001) Different types of repeat expansion in the TATA-binding protein gene are associated with a new form of inherited ataxia. Eur J Hum Genet 9:160–164. CrossRef Medline